Assessment of Mean Glandular Dose in Mammography

A thesis
submitted in partial fulfilment
of the requirements for the Degree
of
Master of Science in Medical Physics

By

Mohammad Zeidan

UNIVERSITY OF CANTERBURY
Te Whare Wānanga o Waitaha
CHRISTCHURCH NEW ZEALAND

Department of Physics and Astronomy
University of Canterbury
Christchurch, New Zealand
2009

Abstract

The mean glandular dose (MGD) was measured for a breast phantom by using molybdenum/molybdenum and molybdenum/rhodium target/filter combinations, at different kVp 26, 28 and 32 kilovolts. The phantom thickness was 7.5cm and was made of BR12 material. The change of dose was studied as a function of depth inside the phantom at different depths from the surface, namely 3.3, 4.3 and 5.3cm, by using TLDs. It was found that the MGD value for different combinations of beam quality (HVL) and energy (kVp) did not exceed the recommended values given by different protocols.

The Mo/Rh target/filter required lower doses to achieve the same or better results compared with the Mo/Mo target/filter. The change in the surface dose as a function of kVp was more significant for Mo/Rh than for the Mo/Mo.

Studying the change in dose within the breast, as a function of depth gives a better understanding of the interactions between radiation and tissue inside the breast. It should be noted that the MGD is a tool for optimization of the mammography parameters. However, the MGD should not be used directly to estimate the risk of determinable health effects from mammography. This will ultimately help to determine limits for the breast surface dose and a better understanding of cancer risk.

In future work, we will try to measure the change of the dose as a function of depth by using more kVp, HVL, different breast composition and different target/filter combinations to give a wider picture for different situations.

Acknowledgments

I would like to express my thanks to all the people who have been helpful during the time it took me to write this thesis.

For this research, first I would like to thank Christchurch Hospital, especially the Oncology and Radiology Departments, for providing the equipment needed for this research. Special thanks to Mark Bird and Wen-Long Hsieh from the Oncology Department, for providing the TLDs and the TLD-reader and assisting me in using these devices which increased my practical knowledge and allowed me to use the reader after their work hours, which ended with some funny stories. Thanks to both of them for informing me of the time required to prepare the detectors due to the number of the TLDs and the calibration process at different energies. Because of these time requirements, my measurements were restricted unfortunately to these different energies, otherwise I would have tried to use more energy values.

A special thank you to Andrew Blair (Medical Physics Registrar, Christchurch Hospital) for all the help and generosity he provided to run the mammography machine during his own time, do the measurements with the ionization chamber and reply to all my e-mails instantly, many thanks.

I wish to thank my supervisors, Lou Reinisch and Samir Abdul-Majid for the meetings and the discussions about my ideas and for replying to my e-mails with more guidelines to ensure the idea was clear.

Other special thanks go to my supervisor, Juergen Meyer, for all the help with the academic writing. He was always there to meet and talk about my ideas, to proofread the chapters, and to ask me questions to help me think through my problems.

Last, but not least, I thank my family: my parents, for giving me life in the first place, for educating me with aspects from both the arts and sciences; for their unconditional support and encouragement to pursue my interests, even when the interests went beyond the boundaries of language and geography. I thank my wife, for sharing her experience of the dissertation writing endeavor with me, for listening to my complaints, for believing in me and for reminding me that my research should always be useful and serve good purposes for all humankind. Lastly, I thank my son, for giving me the most beautiful hugs and smiles in the world every morning and the motivation to succeed.

Contents

List of Figures

List of Tables

1 Introduction

Cancer refers to a group of diseases in which cells in a part of the human body grow abnormally. The common factor for different types of cancers is that they all start when cells grow out of control. Untreated cancer can lead to death because breast cancer is a malignant tumor, which usually starts from the mammary glands in the breast [1].

Breast cancer is the most common cancer among women all over the world [1-4]. According to the American Cancer Society, the chances of an American female developing breast cancer in her life time, are about 12% [2]. The New Zealand Breast Foundation shows that the average risk of a New Zealand woman to be diagnosed with breast cancer in her life time is 11% [1, 3, 5].
In general, most breast cancer societies confirm that breast cancer is the second leading cause of death of all cancer types for women [1-3, 5].

Researches agree that early detection of breast cancer can save many lives every year [1-2]. However, as for other cancer types, breast cancer is detected after symptoms appear in the later stages because, in most cases, there are no symptoms of the disease during the early stages. To detect the disease, a screening test such as a mammogram is recommended to find the cancer before the symptoms appear [1-2, 5].

Mammography refers to the x-ray examination designed specially for detecting human breast pathology [6]. Breast screening relies on mammography to detect

cancer in its early stages due to small changes in tissue composition. As with any examination that includes x-rays, there is always a small stochastic risk of inducing cancer. It is therefore important to evaluate the risk from the dose delivered to the patient during the screening process [7]. In other words, to keep the dose as low as reasonably achievable (ALARA) [6, 8-9].

Accurate dosimetry of the dose delivered to the breast during the screening process has been of interest to a number of investigators [10-11]. The dose delivered to the breast can be estimated by measurements on patients or in most cases by using a phantom. The dose delivered to the breast depends on: the x-ray spectrum (target/filter) combination; breast composition (a ratio of glandular tissue to fat tissue); breast thickness and the kVp value [7, 12-15].

Because of the low energies used in mammography, typically in the range between 25-35 kVp during screening, the dose within the breast will decrease rapidly as the depth increases. This requires using a quantity to represent the risk from using x-rays on the breast. In other words, this quantity needs to represent the dose delivered to the whole organ (breast) [16-17].

Mammary glands are considered to be the most radiosensitive part of the breast [17-19]. Therefore, measuring the mean glandular dose (MGD) within the breast is the recommended quantity to evaluate the risk from radiation to the breast. MGD is a quantity that represents the average dose delivered to the breast. It cannot be measured directly because it depends on the kVp of the x-ray tube; target/filter combination; breast composition and breast thickness [7, 13, 18].

The quantities required to find the MGD is the normalized glandular dose (D_{gN}). This represents the dose delivered, per unit of entrance surface exposure (X_{ESE}), for a given beam quality (HVL); breast composition; breast thickness and kVp [4, 6, 10-12]. It also needs to be taken into consideration that the D_{gN} values vary depending on the target/filter combination used in mammography unit [13, 15, 19-21]. The D_{gN} values are available in standard tables depending on all the above factors 20-21].

Investigators also study the relationship between the surface dose and the dose, as a function of depth, within the breast as one of the methods to determine the risk of mammography [16]. The entrance surface dose can be determined by measuring the x-ray output with an ionization chamber. To estimate the dose inside the phantom (breast) at different depths, dosimeters, such as thermolminescent dosimeter (TLD), need to be used [16-17].

In this research the phantom that will be used to estimate the dose delivered to the breast is a phantom made from BR12 material [15-16, 21]. This phantom has the standard breast composition (50% glandular tissue/50% fat tissue) and 7.5cm thickness. Different target/filter combinations will be used: molybdenum/molybdenum (Mo/Mo) and molybdenum/rhodium (Mo/Rh) and different kVp: 26, 28 and 32 kilovolts will be applied for both target/filter combinations.

This research also includes finding the change in dose, inside the phantom (breast), as a function of depth, by placing the TLDs inside the phantom at different depths: 3.3, 4.3 and 5.3cm which were chosen because of the set up of the phantom slabs. Measuring the change of the dose, as a function of depth within the breast, gives a

better understanding of the change in dose inside the breast, depending on the kVp, target/filter combination and beam quality [16]. In addition, measuring the surface dose and the change of dose with the depths helps to determine limits for the breast surface dose and a better understanding of cancer risk.

2 Background

In this chapter some basic background information is provided. First I will briefly describe the breast anatomical structure with a few little more details about the mammary glands. This will be followed by discussing the structure of the mammography unit with more details about the x-ray tube and the compression paddle. Finally this chapter will discuss the *in vivo* dosimetry for the breast.

2.1 Breast Anatomy

In order to know the changes that can happen to the breast under abnormal situations, it is important to know the anatomical structure and constituency of the breast [23].

In general, a mature female's breast is composed of glands and fat. The human breasts do not contain bone or muscles [18, 23]. Each breast has a nipple where the ducts of the mammary glands open onto the body Figure 2.1. The most important anatomical part of the breast is the mammary glands, which are common in both sexes [23]. However, for males these glands remain rudimentary and functionless [7].

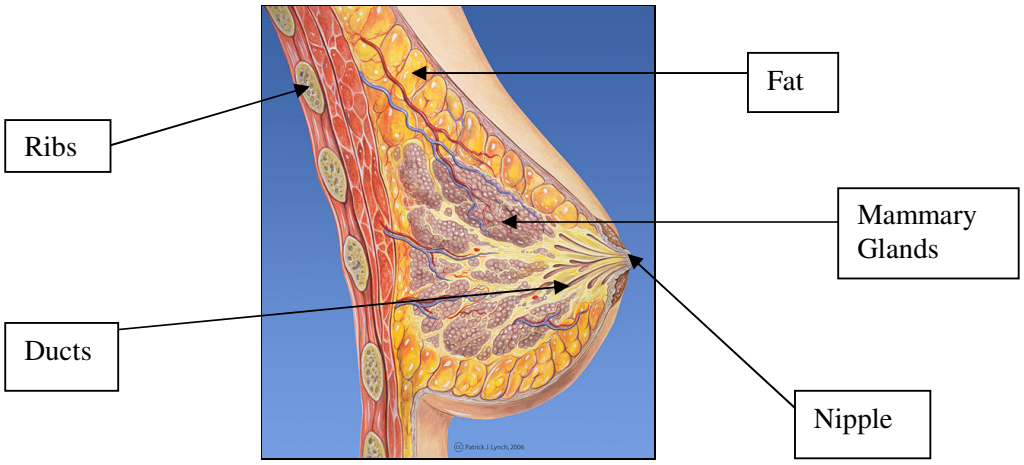

Figure 2.1: Breast normal anatomy cross-section view [24]

The main function of the female breast is to produce milk for the newborn. The mammary glands produce the milk from water and nutrients taken from the bloodstream [23]. Figure 2.1 shows the ducts, which work as contact channels between the mammary glands and the nipple. Internally, the breast structure is the same for all females, only the size and shape of the breast varies [23-24].

The size and shape of the breast may change over time due to, for example, the menstrual cycle, pregnancy and age [23-24]. Some women have more mammary glands in their breast than others: this is mostly correlated with age where younger women have more mammary glands than older women. Some women have more fatty tissue or more connective tissue, which makes the breast more firm [7, 23-24].

The main subject of this research, from a medical physics point of view, is the mammary glands as they are the most sensitive part of the breast and are vulnerable to cancer. These glands are also highly responsive to hormonal changes [23]. According to Frederic H. Martini, "mammary glands of the breast are anatomically related to apocrine sweet glands. A complex interaction between sex hormones and pituitary hormones controls their development and secretion." [23]

The anatomical structure of the breast is mostly fat, unlike other parts of the body. Studies of the breast require images with maximum visualization of the breasts' anatomy to detect a non-palpable cancer [18, 23]. When using ionizing radiation for such an organ containing sensitive glands, it must be optimized to avoid increasing the chances of inducing cancer in the patient [18, 25]. X-ray mammography is one of

the most effective techniques used to detect, diagnose and show a variety of breast diseases. Mammography is designed to detect breast pathology [7, 18, 25].

2.2 Mammography

Mammography is studying and imaging the breast, using images created with x-ray radiation [6-7, 18]. The x-rays used for mammography show the fibrous, fatty and glandular tissues of the breast. The actual test is known as a mammogram. There are two types of mammograms [18]. Firstly, a screening mammogram which is used for women with no symptoms of breast cancer, to detect any cancer in its early stage. A screening mammogram, can be done from two different angles: oblique (from the side of the breast), and a craniocaudal (from above the breast) [18, 26]. Secondly, a diagnostic mammogram the purpose of which is to evaluate an existing problem, such as a discharge from the nipple or a lump [26].

X-ray mammography is a radiographic examination designed to detect breast pathology. The objective of a radiographic examination is to produce an image with maximum visualization of the breast's anatomy for both normal and abnormal tissues (signs of disease) [18, 26]. Mammography is considered the best radiographic examination to meet this objective. This is because mammography uses a low energy radiation dose as the attenuation differences between a normal tissue and a cancerous tissue increases rapidly with the lowest x-ray energies [6, 26, 27].

Mammography uses low kVp with either a molybdenum (Mo), Rhodium (Rh) or Tungsten (W) target in the x-ray tube coupled with specialized beam filtration. Figure 2.2 shows the design of a mammography machine [18].

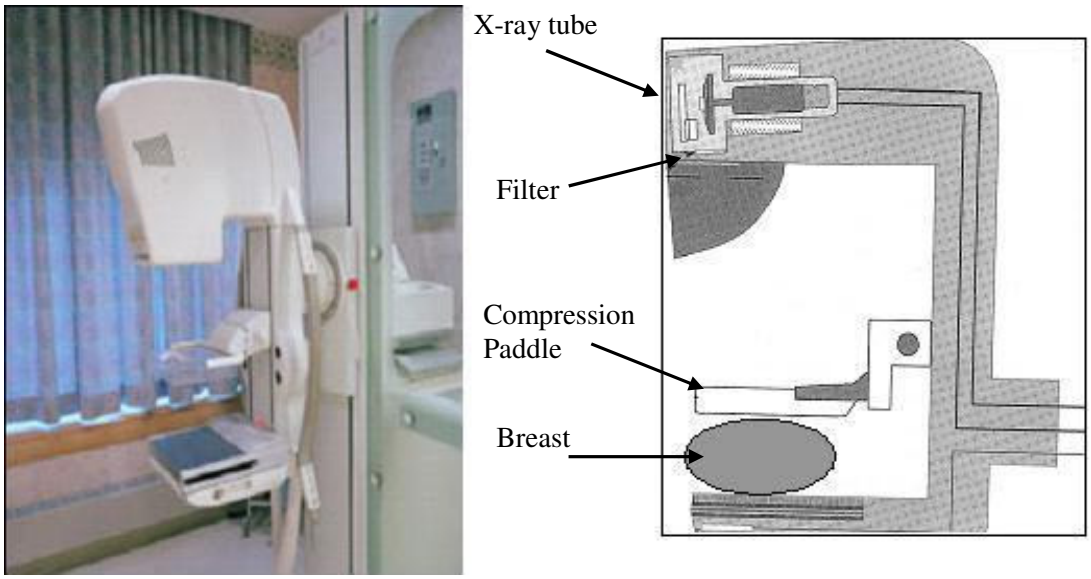

(a) **(b)**

Figure 2.2: Mammography Machine. (a) a picture of a real mammography machine [28] (b) same machine from inside showing the x-ray tube, filter, collimator and compression paddle [18].

A mammography machine has two major components that make it more effective and sufficient for breast screening than any other radiographic machines. These two components are, the types of x-ray tube i.e. target/filter combination and the compression paddle.

In mammography, the doses to the patients are small and do not reach the threshold for determining risk effects. The probability of the occurrence of stochastic effects is also small. However, the probability of stochastic effects occurring increases as the absorbed dose increases [27, 29]. To achieve the optimal x-ray energy with mammography requires the use of a specific x-ray target material to generate a characteristic x-ray of the desired energy and the use of a filter to attenuate and remove the undesirable low and high x-ray energy, caused by the Bremsstrahlung spectrum [18, 30-31]. Doses to the patient can change depending on the choice of the x-ray tube used (target/filter) and the breast characteristics (thickness, density, etc).

2.2.1 X-ray tube

The most common material used for the anode in the mammography x-ray tube is molybdenum (Mo) with (Z=42), although one can find rhodium (Rh) with (Z=45) and tungsten (W) with (Z=74) in some machines [18]. The characteristic x-ray production of molybdenum and rhodium is the reason for choosing these two materials as the anode material. These materials are more commonly used world-wide in mammography machines rather than tungsten [7, 18].

Using molybdenum and rhodium within the x-ray tube has the great advantage of achieving the required radiographic contrast with the soft breast tissues because of their lower atomic number compared with that of tungsten. They produce major characteristic x-ray peaks at 17.5 and 19.6 keV for Mo, and 20.2 and 22.7 keV for Rh. Figure 2.3, shows the process of producing Bremsstrahlung and characteristic radiation for a molybdenum target [16, 18].

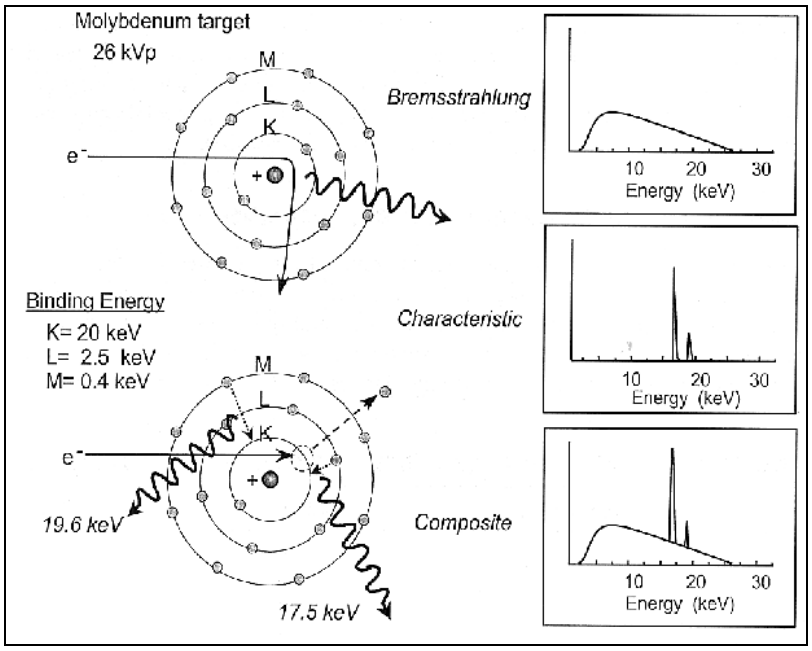

Figure 2.3: The output of the (Mo) x-ray system is composed of bremsstrahlung and charateristic radiation [18]

One of the common filter materials used in mammography is the molybdenum filter with a (30µm) thickness, which can be used in combination with a molybdenum target (Mo/Mo). The rhodium filter is another one with a (25µm) thickness and can be used in combination with the molybdenum target (Mo/Rh). Also, the rhodium filter can be used with the rhodium target (Rh/Rh) [18, 33-34]. The reason for having the filter with the x-ray tube is to reduce the low energy x-rays and the high energy X-rays so they are not incident upon the patient [18] as Figure 2.4 shows.

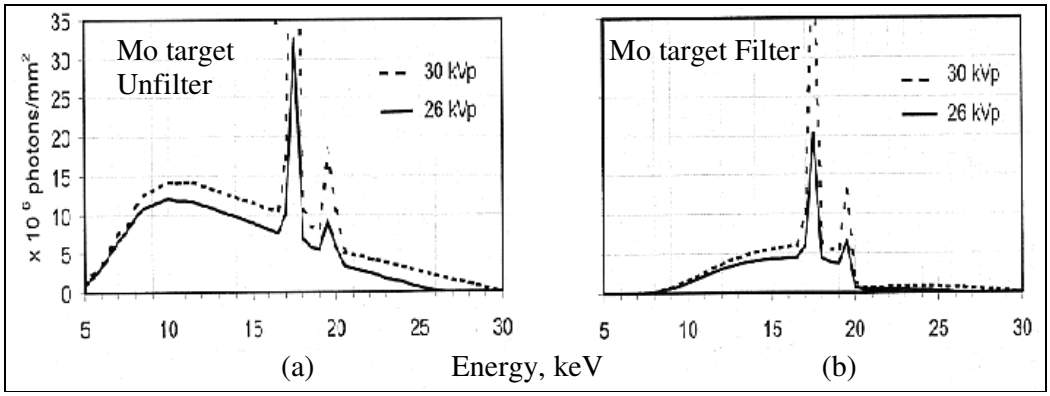

Figure 2.4: (a) Unfiltered spectra from a Mo target contains a relatively large fraction of low- and high energy, (b) filter spectra from a Mo target where the filter terminates the majority of the low- high energy [18]

2.2.2 Breast Compression

The compression of the breast during a mammogram is a very important part of the examination process because it helps improve the quality of the mammogram [18, 34-36]. The compression of the breast is facilitated by using the compression paddle where the breast is placed between two parallel flat plates. One of these two plates is moveable to produce a force over the breast. The main idea of this compression is to reduce the breast thickness and this will give the x-ray the chance to penetrate the breast more uniformly [34], as shown in Figure 2.5.

The benefits of breast compression during screening or diagnosis are [18, 34]:

- Immobilizes the breast to eliminate blurring of the image caused by motion.

- Reduces x-ray scatter and increases the contrast.
- Increases the sharpness of the picture and reduces the geometric blurring.
- Allows the use of a lower x-ray dose since a thinner amount of breast tissue is being imaged

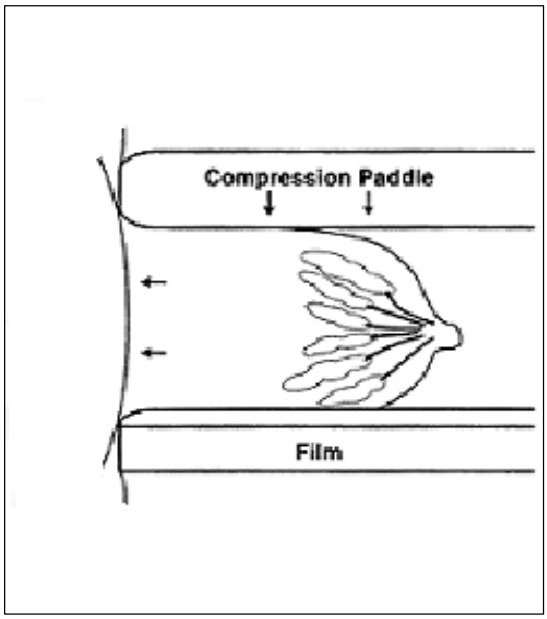

Figure 2.5: Standard mammography views are taken first [37].

2.3 Breast Dosimetry

Detecting cancer in the mammary glands in its early stages increases the chances of recovery [7, 18]. However, the mammography, compared to other conventional x-ray machines, has the advantage of using target materials with low atomic numbers and because the operated energy range for mammography units is 25-35 kVp, the image quality and the energy of the x-ray used, needs to be taken into consideration [18]. In other words the main goal is to have high image quality to maximize the detection of abnormalities and to give a low dose to minimize cancer induction [26, 27].

As with any technique based on ionizing radiation, there is a small but a real significant risk of radiation to induce a tumor [7]. Thus the mammography machine, while having the potential to detect cancer, can also increase the cancer incidence in the radiosensitive tissue during the examination [38]. According to (ICRP, 2007) the breast has 0.12 tissue weighting factor for the effective dose examination [39].
Therefore, it is necessary to evaluate (optimize) the dose delivered to the breast or to any other organ in the body to minimize the risk of radiation induced cancer [7, 26]. Optimization will increase the benefit/risk ratio for the diagnostic procedure [7]. The benefit term from this ratio, presents the improvements on the diagnosis procedure, whereas the risk expresses the hazard from exposing the patient to an ionizing radiation, which always needs to be minimized [7, 26-27].

Using the term *in vivo* in the diagnostic process refers to measurements of the dose delivered to the patient during the treatment or the diagnostic examination [7, 40-41]. This measurement can be taken by placing the measurement instruments on the skin

or inside the patient very close to the target [7, 40]. In the absence of the patient these instruments are placed on a phantom. *In vivo* dosimetry gives a better understanding of the benefit/risk ratio and checks the behavior of the medical device (mammography) [40-41]. Knowledge of the actual dose delivered to the breast depends on: the characteristics of the equipment (x-ray tube target/filter, beam quality) and on the size of the breast/phantom composition [16, 40].

Finding the mean absorbed dose to mammary glands is the preferred measure to express the radiation risk of mammography [7, 16, 42]. Before choosing mammary glands there were different trials to measure the breast dose. For example Boag et al, 1976 considered using the total energy imparted on the breast [7]. The relative risk was determined from the measurements of depth dose curves or entrance and exit doses [7]. The National Cancer Institute NCI, (1977) [43] suggested using the mid-breast dose to measure the radiation risk to the breast. But none of these trials gave enough details about the breast dose [7].

In 1976, Karlsoon in his article, "Absorbed Dose in Mammary Radiography" suggested that finding the mean dose of the mammary glands would be more useful as a measurement of the risk [7]. His suggestion was based on the anatomical structure of the breast and the energy absorbed by it, as the mammary glands are the part of the breast most sensitive to radiation. A few years later, the International Commission on Radiological Protection (ICRP, 1987), and other protocols (European protocol, the British Institute of Physical Sciences in Medicine (IPSM 1989, 1994) [7, 14] supported Karlsoon's suggestion and recommended using the mean glandular dose (MGD) as the most appropriate quantity to represent the radiation risk to the breast [7, 17].

Accurate assessment of the surface exposure levels is considered a first step [16]. Additionally, the relationship between the surface exposure and the absorbed dose to tissue, as a function of depth, is also important [16-17, 44]. The breast surface exposure is typically translated into a mean glandular dose (MGD) to access the radiation risk within the mammary glands [7, 10, 12-13]. Thus, the mean glandular dose (MGD) can be defined as the quantity used to express the absorbed dose by the breast to estimate the radiation risk [7, 10]. However, even with the agreement of using MGD as a measurement of the radiation risk to the breast, measuring the MGD directly, is currently not measurable because these glands are located inside the breast [7, 10, 16]. However, the MGD can be determined indirectly by two methods [7]:

1. A breast phantom
2. Direct surface measurements on the patient

In this research, a breast phantom was used to determine the MGD.

2.4 Overview of approach

This chapter discussed some points briefly, and others in more detail: female breast structure and the effect of the mammography radiation on the breast. The mammography unit structure and why it is considered the best unit, using ionizing radiation to detect breast cancer at the early stages. In the next chapter, materials used in this research will be characterized and the method followed for doing the measurements.

3 Materials and Methods

In this chapter we will discuss the equipment used in this research: the mammography unit, thermoluminescence dosimeters (TLD), phantom and the ionization chamber. Also, the second part of this chapter will show the experimental method (preparation process) for the TLD and the phantom.

3.1 Mammography Unit

All the experiments described in this research were performed using the Siemens Nova 3000 mammography unit [45], shown in Figure 3.1. Either a molybdenum/molybdenum (Mo/Mo) or a molybdenum/rhodium (Mo/Rh) anode/filter combination was used. The voltage range of the x-ray tube mammography unit is from 23-35 kVp, and the maximum field size is (18 X 24) cm^2.

Figure 3.1: MAMMOMAT 3000 Nova [45]

3.1.1 Thermoluminescence Dosimeter

The use of thermoluminescence dosimeters (TLDs) has been accepted in all areas of the radiographic imaging (x-ray) as one of two dosimeters types: (a) integrating dosimeters such as TLD optical dosimeters, and (b) electrical conductivity dosimeters such as semiconductor dosimeters [46-47].

A TLD is a phosphor on a solid crystal structure such as lithium fluoride (LiF), lithium borate ($Li_2B_4O_7$) or calcium fluoride (CaF_2). The most commonly used TLD is lithium fluoride (LiF) because of its high stability and its response to a wide range of energies used with mammography [47-48]. Also, lithium fluoride has the advantage of being very close to tissue equivalent due to its atomic number ($Z_{eff} \approx 8$) compared to 7.5 for tissue [46-48].

After being irradiated, heating these crystalline materials is followed by the emission of visible light proportional to the amount of the radiation they are exposed to (absorbed dose). This emission of light with the application of heat is known as thermoluminescence. Measuring this amount of emitted light estimates the radiation dose delivered to these crystals. This technique is called the Thermoluminescence Dosimeter (TLD) [47-48].

When TLD materials are exposed to ionizing radiation, electrons are raised to higher energy levels in the atoms of the TLD. Most of these electrons will return to their original state. Some of them become trapped in the higher energy levels. Upon heating, they return to the ground state together with the emission of light. This light is what is usually measured as an expression of the amount of the radiation absorbed. However, some of these electrons will stay (trapped) in the higher energy levels [47].

Experimentally, after irradiating LiF crystals, they are inserted into a heater "TLD-reader" where a photomultiplier tube (PMT) converts the emitted light from the TLDs into an electrical signal that can be measured. Drawing the light emitted as a function of time, produces a so-called "glow curve" [46-48].

The glow curve shows peaks, where each one of these peaks represents a different trapped energy level, and the area under the glow curve is used to measure the delivered dose [47-48, 50-51] as shown in Figure 3.2.

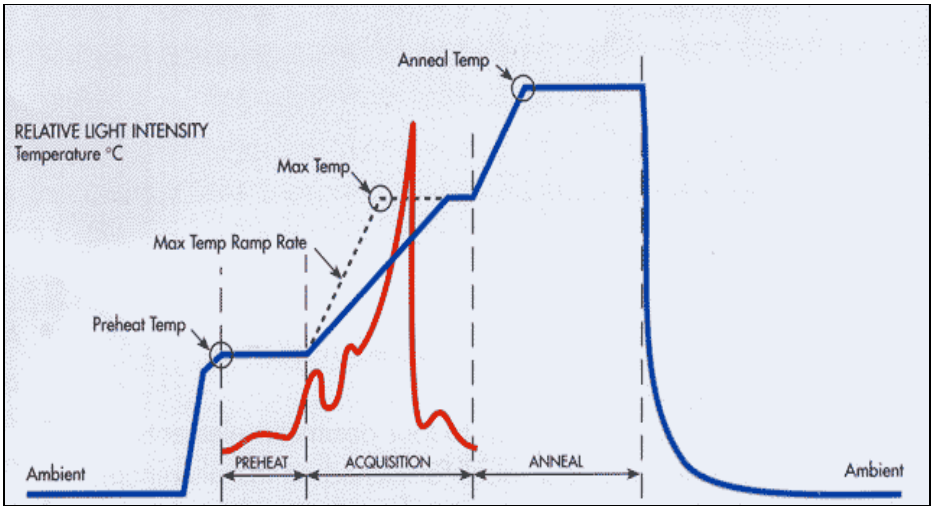

Figure 3.2: Time-temperature profile and glow curve for LiF: Mg, Ti (TLD-100) [49]

Thermoluminescence dosimeters come in many different shapes (powder, chips and rods) and in different sizes. There are many advantages of using TLDs for measuring dose, especially with mammography. Some of these advantages are [47-48, 50-51]:

- Its small size makes it easy to use in many positions within the human body or in phantoms
- TLD (LiF) can be used to measure a wide range of dose 10^{-5} – 10^{3}Gy

TLDs are used for measuring the absorbed dose. The importance of measuring the absorbed dose from a diagnostic point of view, comes from [7]:

- Reducing the patient dose by improving the equipment design.
- Improving the radiographic techniques as part of reducing the patient dose.

However, there are some disadvantages of TLDs: one is the lack of uniformity (different TLDs have different sensitivities and this requires a group calibration or an individual calibration). Due to this lack of uniformity, TLDs must be calibrated before being used especially this study will be using two different target/filter combinations and may case small difference with dose measurements. Ionization chambers are mostly used to calibrate TLDs [46-48].

The ionization chamber will be placed at the same effective point of the measurements and exposed to the same dose the TLDs are exposed to. This makes the energy responses not an issue because they were calibrated at the same energies where the measurements were taken [16, 40, 46].

The disadvantage of the TLD is the time it needs in the annealing process (preparing for use). It is a compulsory step with TLDs before use. Annealing is resetting the TLDs by heating them to a high temperature reaching 400^{o}C, in which all the dosimeters are placed in a TLD oven and exposed to heat for 2 hours followed by another 2 hours at (100^{o}C) to release trapped electrons on the TLDs. This process can take up to 5 hours [46].

The type of TLD used in this research was a Harshow (TLD-100) with a lithium fluoride base with Mg:Ti doped (LiF: Mg:Ti). The TLDs were 3.1 × 3.1 × 0.9 mm^3 and were chip-shaped. They were all used to measure the dose in different depths inside a phantom, as described in the next section.

3.1.2 The Phantom

A phantom is a tissue equivalent material corresponding to the organ of interest (breast in this study). It reflects the following characteristics: linear and mass attenuation coefficient, mass absorption coefficient, energy distribution, size and shape. The advantages of the phantom measurements are [7, 53]:

- Results are more reproducible
- No interference with patient examinations

There are a few requirements the phantom must have, to be considered as a suitable phantom to simulate the breast [7, 53-54]:

- Composition of the breast (percentage of the glandular tissue to fat tissue)
- Sensitive to small variations (temperature and pressure)
- Easy to use
- Solid and large enough to provide appropriate scatter conditions
- Ability to change thickness

In general, phantom measurements give a better understanding of the dose level applied under different conditions and help to assess the effects of the machine performance, such as the dose output [7, 54-55]. Also, using the phantom helps comparison between different x-ray tubes depending on the size, shape, and composition of the breast (ratio of mammary glands to fat tissues) [7, 52, 54].

The phantom used for this study represents the female breast and is called tissue equivalent phototimer consistency testing slabs (Model 014A) by Fluke Biomedical Company, Virginia, United State of America [55]. It resembles a compressed situation and standard granularity with a tissue consisting of 50% fatty tissue and 47% glandular tissue [7, 16, 34-35, 40]. This phantom is made from a material known as BR-12 or BR50/50 [7, 16]. The phantom is shown in Figure 3.3. This phantom is designed to be in slabs (rectangular shaped) 12.5cm length, 10cm width, with different thicknesses of 2, 1, and 0.5cm [55]. This is to makes it easier to study the dose delivered to the breast as a function of depth.

Figure 3.3: Tissue equivalent phototimer consistency testing slabs (model014A) [55]

3.1.3 Ionization Chamber

The ionization chamber is the best option to use in the calibration process for the TLDs [16, 40-41]. In this research the ionization chamber used was model 96035B dual entrance window parallel plate with a flat response suitable for both diagnostic and mammography. It was made by Supertech Company, Elkhat, United States of America [56]. One of the entrance windows is used for Mammographic measurements see Figure 3.4. The dimensions of the ion chamber were 6.35±0.04cm diameter by 1.33±0.01cm thickness, where the wall is made of graphite-coated acrylic [56]. The ionization chamber was placed on the surface of the phantom to measure the entrance dose for different kVp from different x-ray target/filters, Mo/Mo and Mo/Rh with take inconsideration the compression paddle placed on top of the chamber to avoid all the backscatter.

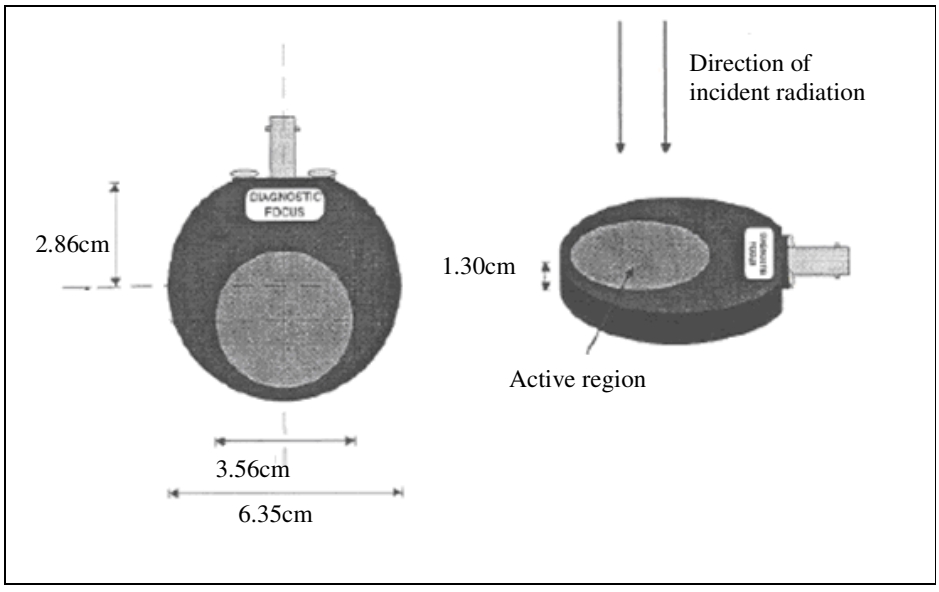

Figure 3.4: The model 96035B ion chamber [56]

3.2 Experimental Method

3.2.1 Thermoluminescence Dosimeters (TLD)

3.2.1.1 Preparation

Before using TLDs they must be kept in a TLD keeper to avoid any damage (scratches, touching by hands). The TLD-keeper is a box that stores TLDs separately with a specific coordinate (row and column) as shown in Figure 3.5. The TLD keeper used in this research could hold up to 50 TLDs.

	1	2	3	4	5	6	7	8	9	10
A										
B										
C										
D										
E										

Figure 3.5: The TLD keeper with the coordinates

Preparing the TLDs for use starts with the annealing process, which is a compulsory step for all TLDs that are going to be exposed to radiation [46-48]. After TLDs are exposed to a known dose of radiation they have to be calibrated to make sure that all the dosimeters will have an equal dose response and sensitivity [46-48]. The calibration of the TLDs is followed by a pre-read annealing. Finally an automatic TLD-reader is used to read the measurement detected [46-48].

It is recommended to keep the time short between the annealing process and irradiation of the TLDs to minimize the effect of background radiation [46].

3.2.1.2 Group Calibration

Because this research studies the dose as a function of depth we must have many of the TLDs divided in groups to cover all depths. It is easier to do the calibration of the dosimeters as a group (batch). All the groups were classified depending on the energy used and the depth, but each group was exposed to the same field size.

The calibration process resulted in a group of TLDs that had an equal dose response and sensitivity. The standard deviation of all readings was within ±3% [46].

3.2.1.3 Pre-read Annealing

Pre-read annealing is the first step in the reading process (read out) for the TLDs, and it immediately follows the irradiation of the TLDs [46]. In this step the TLDs are carefully removed from the TLD-keeper and are placed on the TLD oven tray (capacity 50 TLDs). The TLDs then need to be placed in small cylindrical holes on the disk to avoid losing one of the dosimeters due to the fan in the convection oven [46].

This step requires a heating of 10 minutes at 100^{o}C, where the pre-read annealing process will take nearly 40 minutes.

After the pre-read process is finished, the TLDs need to be placed in the automatic TLD-reader in groups to get the TLDs read out depending on the target/filter x-ray tube used, energy used and the depth.

3.2.1.4 The Automatic TLD-Reader

The TLD-reader used in this research was the Harshaw Model 5500 Automatic TLD-Reader, Figure 3.6. Up to 50 TLDs can be placed in the reader where each chip is heated at a rate of 10^{o}C/second, and is exposed to a hot gas stream [46, 48]. The light emitted from the dosimeters is converted, by the low noise in a high gain photo multiplier tube (PMT), into a current that is integrated. This results in the glow curve to give a reading in nanocoulombs (nC) [46, 57]. Each one of the readings is recorded under the name or number of the TLD.

Figure 3.6: Harshaw Model 5500 Automatic TLD-Reader. The left part is where the TLDs are placed and exposed to the gas; the monitor shows the glow curve [57]

3.2.2 Phantom

The phantom used for this study is a compressed phantom with 50/50 composition tissues (glandular/adipose) designed in slabs. The maximum possible thickness of the phantom is 8.5cm but for this study the maximum phantom thickness used was 7.5cm.

The important phantom slab is the one slab that carries the TLDs when they are exposed to radiation. This slab is the thinnest slab of all (0.5cm). It contains 15 holes, each of a cylindrical shape. We took a 5cm distance from the chest-wall edge and arranged all the holes in a matrix (3×5) to cover breast surface area (nipple edge) with a 3mm depth and 0.42mm diameter, as shown in Figure 3.7. These slabs are designed with the holes being at an equal distance from each other, and also symmetrically arranged to compare the dose for side edges and the central part of the phantom.

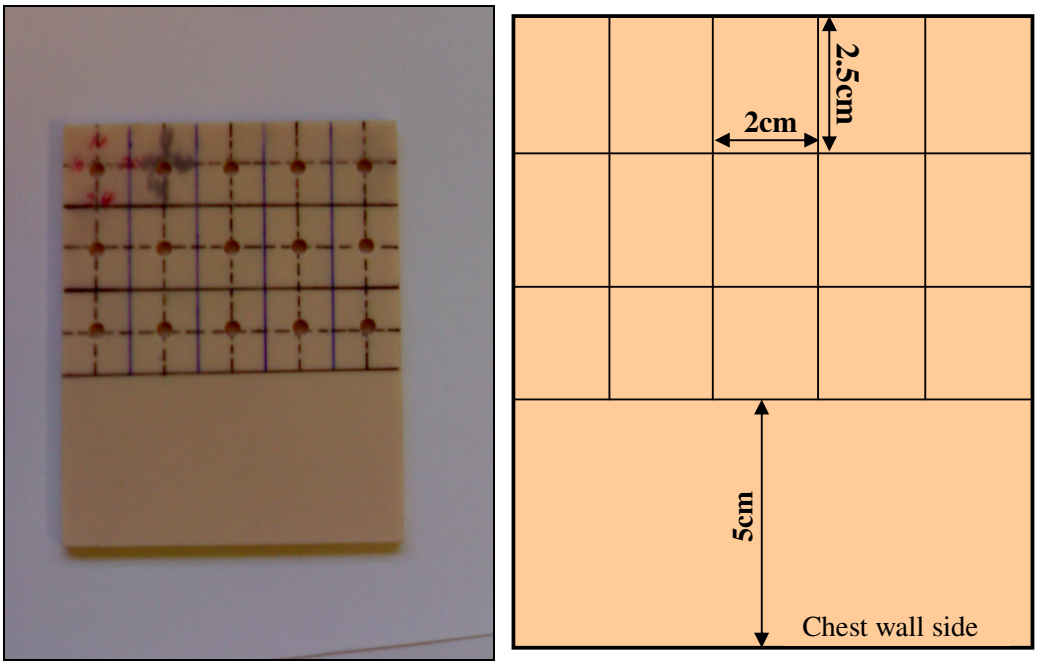

Figure 3.7: The 0.5cm thickness slab, with the mold holes to place the TLDs during the test

Because the TLD thickness was almost 1mm and the hole depth was 3mm, this resulted in a gap of air between the phantom slabs when they were placed on top of each other. This affects the TLD readings because of the increase in backscatter. To avoid or minimize the backscatter, some Perspex, of the same shape and diameter of the holes but with 2mm thickness, was placed on top of the TLDs to cover the gaps, as shown in Figure 3.8. The holes' diameter and the Perspex thickness helped to immobilize the TLDs inside the holes.

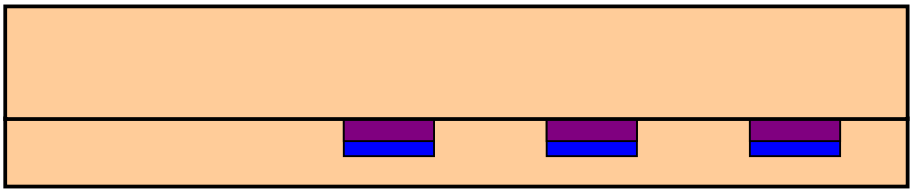

Figure 3.8: The (0.5cm) slab thickness (bottom), have the TLD on blue and the Perspex on purple, covered with another phantom slab (top).

3.2.3 Measurements

It is important to have a suitable phantom that matches the requirements to simulate the organ being studied. In this study, using the breast phantom, there are two ways to carry out dose measurements [7, 58]:

1. Measure the entrance surface dose (ESD) alone
2. Measure the entrance and the exit doses

Measuring just the entrance surface dose (ESD) does not take into consideration the fact that the dose will decrease as the depth increases [19]. However, measuring the ESD and the exit dose has been proven to be more useful. It also includes more details about the variation of the dose and the relation of that to the density of the breast [16, 19, 58]. The second method shows the importance of *in vivo* dosimetry for the patient

or the mean glandular dose (MGD) for the breast [7, 40]. Overall, *in vivo* dosimetry helps improve the accuracy and precision of the dose delivered to the target [40].

However, because of the difficulties of determining the MGD directly due to the location of the mammary glands, there are some protocols such as those in the Institute of Physical Sciences in Medicine (IPSM) (1989, 1994) [7, 21-22, 59] that set out the process to estimate the MGD. The methods of these protocols are based on the fact that the assessment of the surface exposure levels is considered as a first step to determine the MGD [16]. The other point, considered important with finding the MGD, is finding the relationship between the surface exposure and the absorbed dose to tissue, as a function of depth [16].

The MGD is calculated by measuring the entrance surface exposure, X_{ESE}, and multiplying the X_{ESE} with the normalized glandular dose (D_{gN}) [7, 16, 21-22] equation 1 [34-35]. The normalized glandular dose represents the average glandular dose per unit entrance surface exposure. It depends on the breast thickness, beam quality, and breast composition [21-22]. The unit of the normalized glandular dose is typically tabulated in (mrad/R) [21-22] which corresponds to (0.01mGy/R) in SI units.

$$MGD = (X_{ESE}) \times (D_{gN})$$
$$[mGy] = [R] \times [mrad/R] \quad \cdots\cdots\cdots \text{Eq.(1)}$$

Taking into consideration that measuring the X_{ESE} by using the ionization chamber will be by mGy, but keeping the equation units most of the literature used, we convert the ionization chamber reading into (R), where 1R=0.00873Gy.

The beam quality is expressed in half value layers (HVL) which depend on the kVp and the x-ray tube target/filter combinations. The kVps used in this research were 26,

28, and 32 kilovolts. The reason for choosing just three voltage values was because of time constraints, i.e. availability of resources at the hospital.

Beam Quality

The process followed to obtain the HVLs was as follows [34]:

1. Setting the ionization chamber at a distance of 65cm from the radiation source (same distance between the phantom and the radiation source)
2. Collimating the x-ray beam so that the ionization chamber will be fully exposed in terms to minimize the backscatter
3. Placing pure (more than 99.9%) aluminum layers on top of the ionization chamber, starting from the lowest layer thickness (1mm) and measuring the dose
4. Adding another aluminum layer on top of the first one and repeating this step until we obtained half of the first measurement (without any aluminum layer)
5. Adding another layer to find the second HVL value
6. Checking the accuracy, by repeating the measurements again without using any aluminum, to compare with the first measurements
7. Repeating the steps (1- 6) for the different energies used for the two x-ray target/filter combinations

The measurements were then applied to equation 2 [34] to find the HVL for each energy:

$$Calculated \quad HVL = \frac{T_b \ln\left[2K_a / K_o\right] - T_a \ln\left[2K_b / K_o\right]}{\ln\left[K_a / K_b\right]} \qquad Eq.2$$

where,

K_o: Dose measured with no aluminum

T_a: Thickness of aluminum immediately below (K_o/2)

T_b: Thickness of aluminum immediately above (K_o/2)

K_a: Dose measured using T_a

K_b: Dose measured using T_b

The point to consider is that the breast dose varies widely with breast composition and thickness as well as the choice of imaging equipment and radiographic technique. Therefore, there are many different protocols European protocol, the British Institute of Physical Sciences in Medicine and methods designed to facilitate and estimate the appropriate value of the breast dose [7, 14, 16]. Each of these methods uses different phantom materials, phantom thickness, x-ray energies (kVp), x-ray tubes and dosimeters, such as TLD and films. TLDs are the most common dosimeter in most of these protocols [8].

Classified the TLD

The next step was to organize the TLDs needed for the measurements, depending on the depths and the nominal energies from the x-ray tubes.

Initially, the Oncology Department at Christchurch Hospital offered (300) TLDs. These were classified into six major groups depending on the energy (kVp). Each group had 50 TLDs. The 50 TLDs were then divided into 3 smaller groups to be calibrated at 3 different depths 3.3, 4.3 and 5.3cm. The reason for choosing these depths was because the existing different protocols covered only specific depths. For example, the American College of Radiology (ACR) chose 4.2cm; in the United

Kingdom they used 4.5cm and in Australia they used a 5cm depth [8]. The maximum number of the TLDs for each depth is 15, Table 3.1.

Group Name	Depth (cm)	Energy (kVp)	X-ray Tube (target/filter)	Total (TLDs)
A	3.3, 4.3, 5.3	26	Mo/Mo	50
B	3.3, 4.3, 5.3	28	Mo/Mo	50
C	3.3, 4.3, 5.3	32	Mo/Mo	50
D	3.3, 4.3, 5.3	26	Mo/Rh	50
E	3.3, 4.3, 5.3	28	Mo/Rh	50
F	3.3, 4.3, 5.3	32	Mo/Rh	50

Table 3.1: Classified the TLDs into groups depending on the x-ray energy**.**

To study the dose, as a function of depth, using different target/filter x-ray mammography tube at different energies. Table 3.1 shows the calibration process was divided into two groups. The first group was the Mo/Mo target/filter x-ray tube for all energies and depths. The second group was the Mo/Rh target/filter x-ray tube for all energies and depths.

The standard deviation of all readings should be within ±3%. Therefore, all the TLDs with a standard deviation higher than 3% were rejected.

After the calibration process was completed, each group had more than 8 TLDs within the required standard deviation although some groups had 15 TLDs within the standard deviation.

Part of the preparation for measurement was to set up the mammography machine to find the lowest dose that could be detected by the TLDs. To do this the ionization chamber was placed at these depths, and exposed to the same beam. The reading from

the chamber reflects the dose needed to get a readable value from the TLDs at any depth.

For example, if the chamber reading is 100μGy as the lowest dose that the TLD can detect then we should set up the exposure factor to deliver no less than 100μGy exit dose. The reading varies depending on the depth, due to the change of the attenuation through the phantom material.

The initial plan of this research was to obtain measurements using lower energies. Trials were done for an energy of 24 kVp for a Mo/Mo target/filter x-ray tube. Then the dosimeters were placed at different depths. It was however, difficult to detect a signal at the depth of 5.3cm due to the high attenuation. Because of these initial results no trials were done on the Mo/Rh for the same energy, and were not considered in this research.

4 Results

4.1 Calculate the MGD

Calculating the MGD depends on different factors, a few of these factors were not changed in this research i.e. the phantom thickness and composition. Also, part of these factors is the beam quality, HVL, which depends on the kVp and the target/filter combination. Table 4.1 and Table 4.2 show the measured HVLs for Mo/Mo and Mo/Rh target/filter, respectively, as a function of the 3 energies used in this research:

kVp	K_o (mGy)	T_a (mmAl)	T_b (mmAl)	K_a (mGy)	K_b (mGy)	HVL (mmAl)
26	6.88	0.3	0.2	3.39	4.16	0.29
28	8.65	0.4	0.3	3.7	4.43	0.31
32	12.58	0.4	0.3	5.79	6.83	0.35

4.1 : The HVL of 26, 28, 32 kVp for Mo/Mo target/filter mammography x-ray tube

kVp	K_o (mGy)	T_a (mmAl)	T_b (mmAl)	K_a (mGy)	K_b (mGy)	HVL (mmAl)
26	5.19	0.4	0.3	2.43	2.87	0.36
28	6.67	0.4	0.3	3.19	3.79	0.37
32	9.91	0.5	0.4	4.39	5.03	0.41

Table 4.2: The HVL of 26, 28, 32 kVp for Mo/Rh target/filter mammography x-ray tube

The measurements of the HVLs in Tables 4.1 and 4.2 show the relationship between the increase of the x-ray tube voltage kVp, and the HVL for both Mo/Mo and Mo/Rh

target/filter combinations. Figure 4.1 shows this relationship graphically. An increase in kVp requires more aluminum to be used to obtain the first HVL. The estimated uncertainty in this figure is 3%.

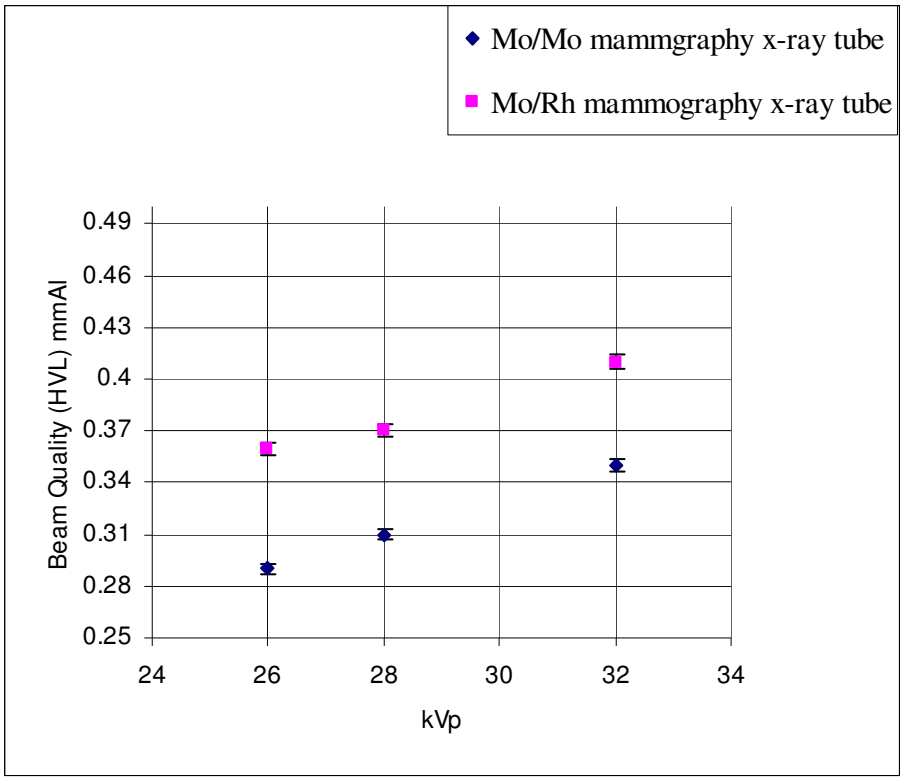

Figure 4.1: The relationship between the x-ray tube voltage (kVp) and the beam quality (HVL) for Mo/Mo and Mo/Rh target/filter mammography x-ray tube

The HVL values at each kVp can be used to determine the MGD. MGD is the mean dose received by the glandular tissue in the whole breast and is an approximation of the actual patient dose [7, 16, 60]. Therefore, MGD is a quantity determine by standard tables with the knowledge of the entrance surface exposure, HVL, target/filter used, breast thickness and composition.

4.1.1 Interpolate the Normalized Glandular Dose

These standard tables are available at Wu X et al [21-22] include the normalized glandular dose values D_{gN} as a function of beam quality, but do not cover the kVp and

the breast thickness 7.5cm used in this research directly. A linear interpolation was used for the relationship between the HVL and the D_{gN} to find the D_{gN} at a nominal corresponding to our phantom thickness and beam parameters. To obtain the correspond D_{gN} for the first kVp in this research 26kVp we must drew the D_{gN} for 25kVp and 27kVp at different HVL for a phantom thickness 7cm from the literature [21] and then find the average of the D_{gN} at each HVL related to 26kVp, see Figure 4.2.

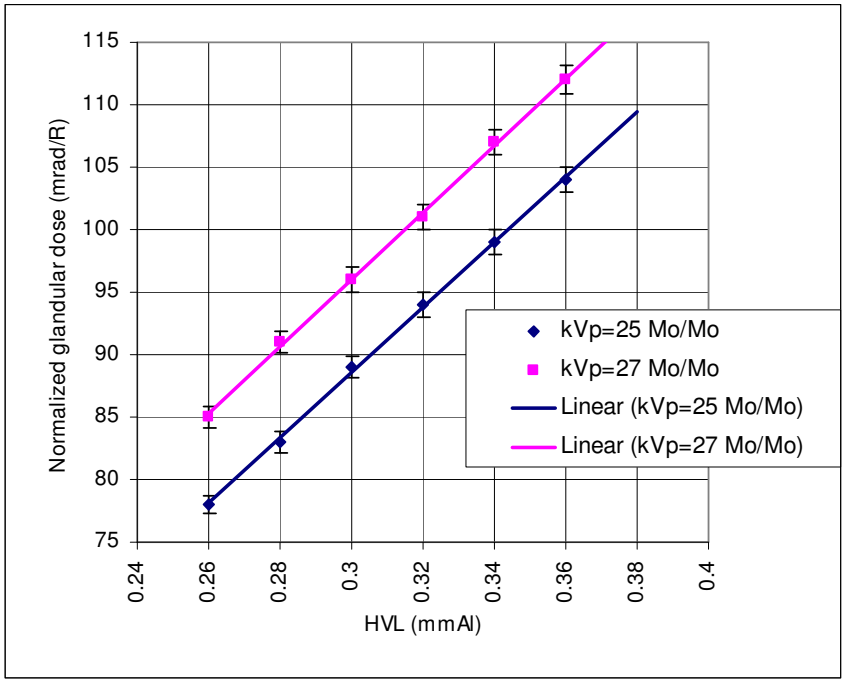

Figure 4.2 : Linear relationship between the HVL and the normalized glandular dose at 25 and 27 kVp with by Mo/Mo target/filter for 7cm breast phantom thickness.

By repeating the same method of the interpolation but for a phantom with 8cm thickness at different HVL for 25kVp and 27kVp, and then finding the average for the D_{gN} for these two kVps we will get the D_{gN} for 26 kVp at these HVL for a phantom with 8cm thickness. Finding the average of the D_{gN} at each HVL for the 7cm and 8cm phantom thickness will end with the D_{gN} for our phantom 7.5cm at different HVL for 26kVp.

For the other kVp values covered in this research the same interpolation method was applied.

Table 4.3 shows these values (interpolated from the literature) at the energies used and HVL measured in this research, and also other thicknesses related to the depths used in this research with more concern with 7.5cm.

X-ray Tube voltage, HVL (mmAl)	Compressed breast thickness (cm)									
	3	*3.3*	*4*	*4.3*	*5*	*5.3*	*6*	*7*	**7.5**	*8*
26 kVp										
0.29	*203*	*189*	*156*	*146*	*124*	*118*	*103*	*82*	**79**	*75*
0.31	*215*	*200*	*165*	*155*	*132*	*125*	*109*	*92*	**86**	*80*
0.35	*238*	*222*	*183*	*172*	*147*	*139*	*121*	*103*	**96**	*89*
28 kVp										
0.29	*205*	*191*	*158*	*149*	*127*	*120*	*105*	*89*	**83**	*77*
0.31	*218*	*203*	*168*	*158*	*134*	*127*	*111*	*94*	**88**	*82*
0.35	*241*	*225*	*186*	*175*	*149*	*141*	*123*	*105*	**98**	*91*
32 kVp										
0.31	*222*	*207*	*172*	*162*	*139*	*132*	*115*	*98*	**92**	*85*
0.35	*244*	*228*	*190*	*179*	*153*	*145*	*127*	*108*	**101**	*94*

Table 4.3: Normalized glandular dose (Dg_N) for Mo/Mo and 50% glandular- 50% adipose breast glandular tissue dose (mrad) for surface exposure of 1R at different breast thicknesses.

The reason for using old units' "milliards (mrad)" and "Rontgen (R)" is because standard tables use these units. This is why they were used in this research. Table 4.3 is adapted from Wu X et al [21].

The values from Table 4.3, were used to study the relationship between the normalized glandular dose D_{gN} and different breast phantom thicknesses i.e. comparing 7.5cm to other thicknesses, for different beam qualities. This relationship is shown in Figures 4.3, 4.4 and 4.5. The uncertainties in the values (polynomial line) were estimated to be within 3%.

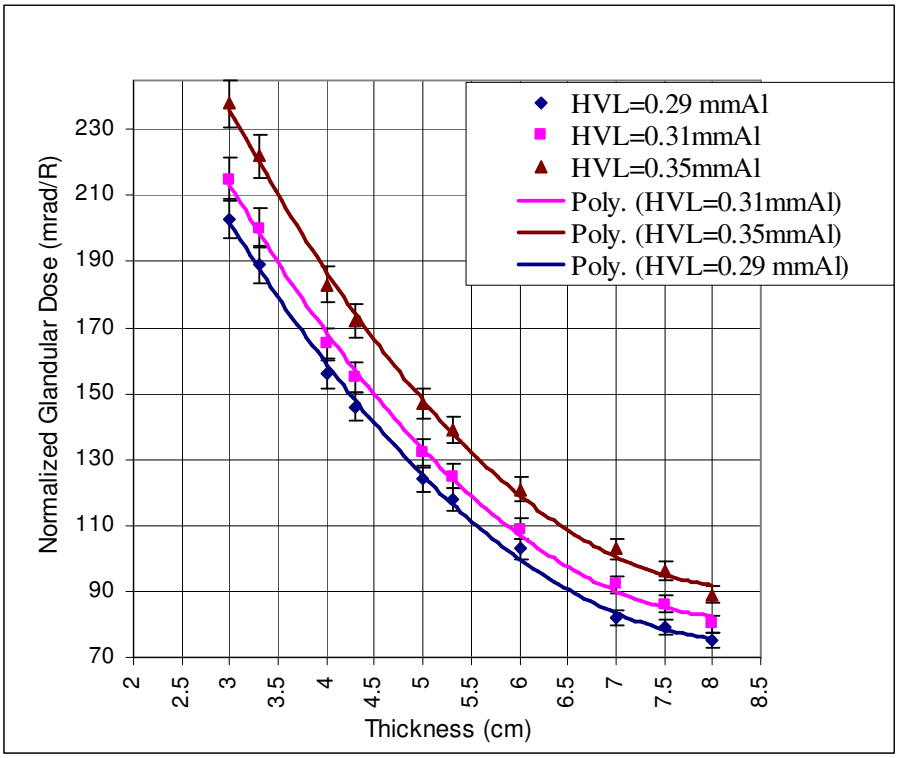

Figure 4.3 : Normalized glandular dose (mrad/R) at 26 kVp for Mo/Mo x-ray tube plotted as a function of depth for three different HVLs (mmAl)

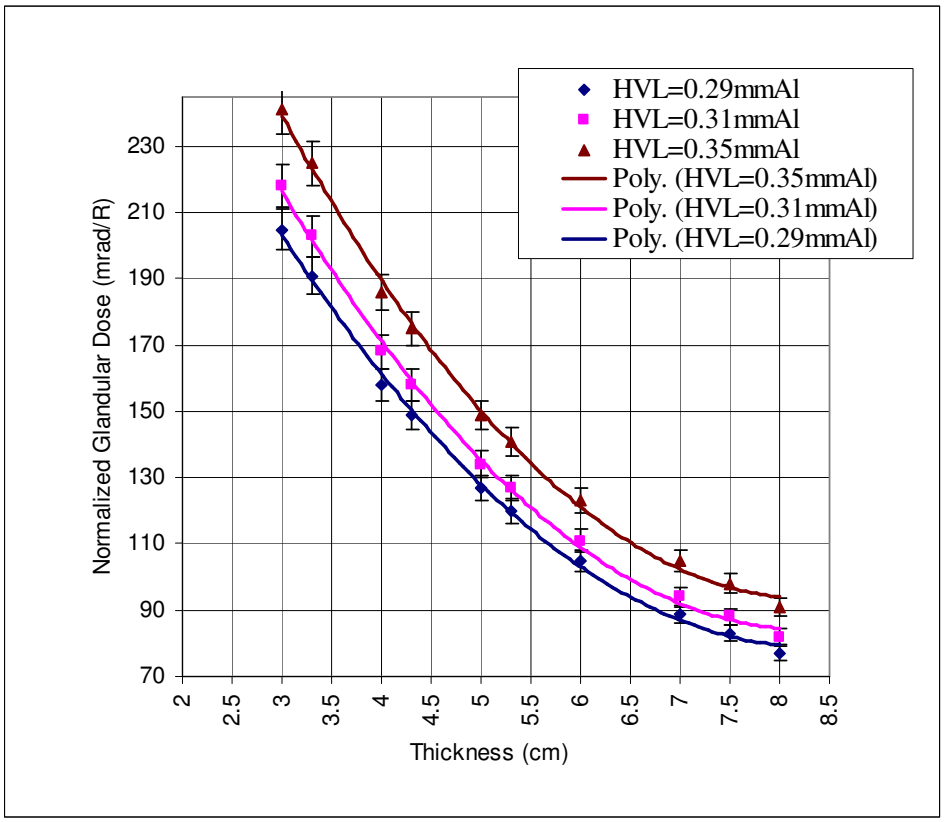

Figure 4.4 : Normalized glandular dose (mrad/R) at 28 kVp for Mo/Mo x-ray tube plotted as a function of depth for three different HVLs (mmAl)

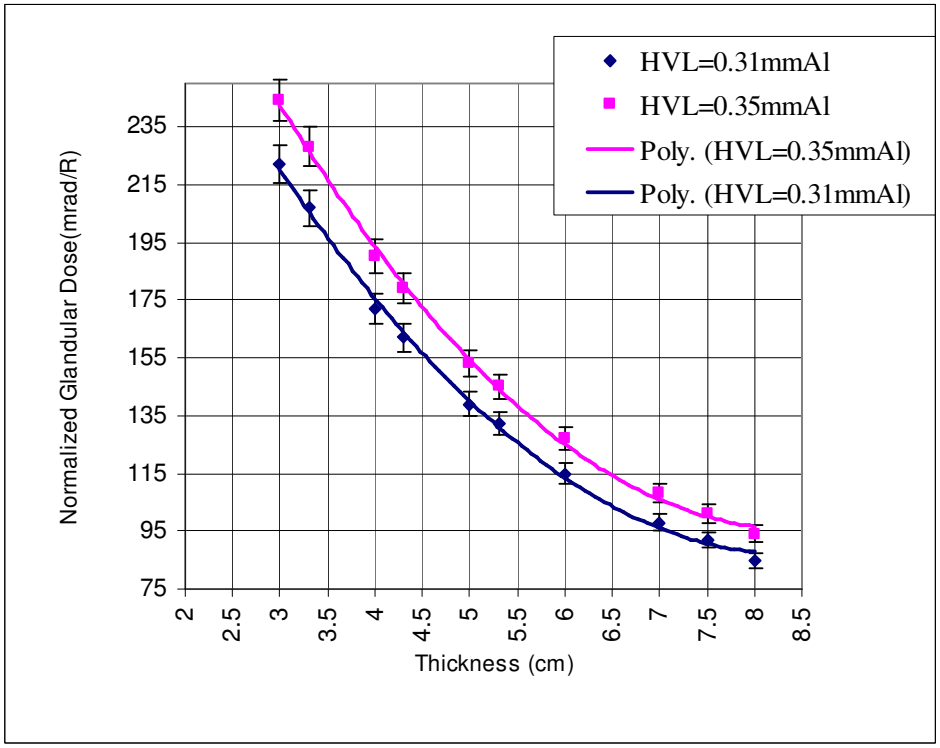

Figure 4.5 : Normalized glandular dose (mrad/R) at 32 kVp for Mo/Mo x-ray tube plotted as a function of depth for two different HVLs (mmAl)

Figure 4.5 shows only 32kVp with Mo/Mo target/filter. That was because no data was available in the literature, relating to the increase on the kVp which requires having more aluminum layers. This leads to an increase in the first HVL value.

The next step was to find the relationship between the normalized glandular dose for a 7.5cm phantom thickness for the Mo/Rh target/filter combination. This required using the standard tables for this target/filter [22]. Table 4.4 shows these values at the energies and different thickness which were done in the same way for Mo/Mo.

X-ray Tube voltage, HVL (mmAl)	Compressed breast thickness (cm)									
	3	*3.3*	*4*	*4.3*	*5*	*5.3*	*6*	*7*	**7.5**	*8*
26 kVp										
0.36	*249*	*233*	*194*	*183*	*156*	*148*	*130*	*110*	**103**	*96*
0.37	*254*	*237*	*198*	*187*	*160*	*152*	*133*	*113*	**106**	*98*
0.41	*277*	*259*	*216*	*204*	*175*	*166*	*145*	*124*	**116**	*107*
28 kVp										
0.36	*251*	*235*	*196*	*185*	*158*	*150*	*131*	*112*	**105**	*97*
0.37	*256*	*239*	*199*	*188*	*162*	*154*	*135*	*115*	**108**	*100*
0.41	*278*	*260*	*218*	*206*	*177*	*168*	*147*	*125*	**117**	*109*
32 kVp										
0.41	*280*	*262*	*220*	*208*	*179*	*170*	*149*	*127*	**119**	*110*

Table 4.4 : Normalized glandular dose (Dg_N) for Mo/Rh and 50% glandular- 50% adipose breast glandular tissue dose (mrad) for 1R at different breast thicknesses.

Table 4.4 is adapted from the standard tables for the Mo/Rh target/filter by Wu et al [22].

Figures 4.6, 4.7 and 4.8, show the relationship between the normalized glandular dose and different phantom breast thicknesses with an uncertainty of 3%, as a function of kVp for the beam qualities measured in this research for Mo/Rh target/filter combination.

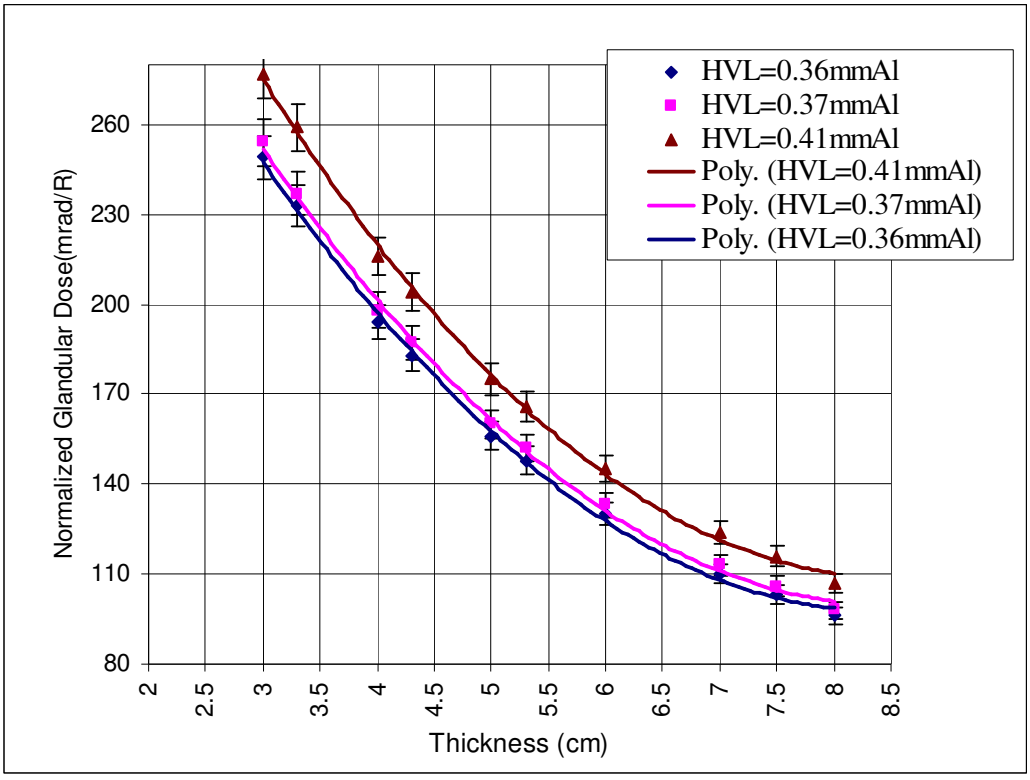

Figure 4.6 : Normalized glandular dose (mrad/R) at 26 kVp for Mo/Rh x-ray tube plotted as a function of depth for three different HVLs (mmAl)

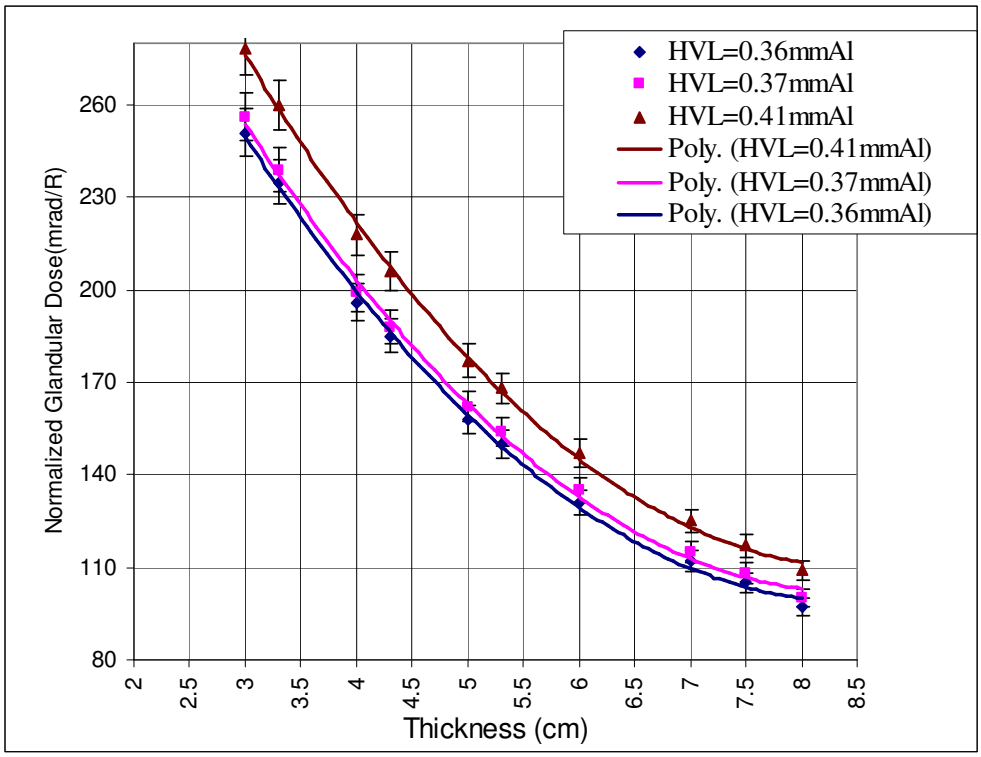

Figure 4.7 : Normalized glandular dose (mrad/R) at 28 kVp for Mo/Rh x-ray tube plotted as a function of depth for three different HVLs (mmAl)

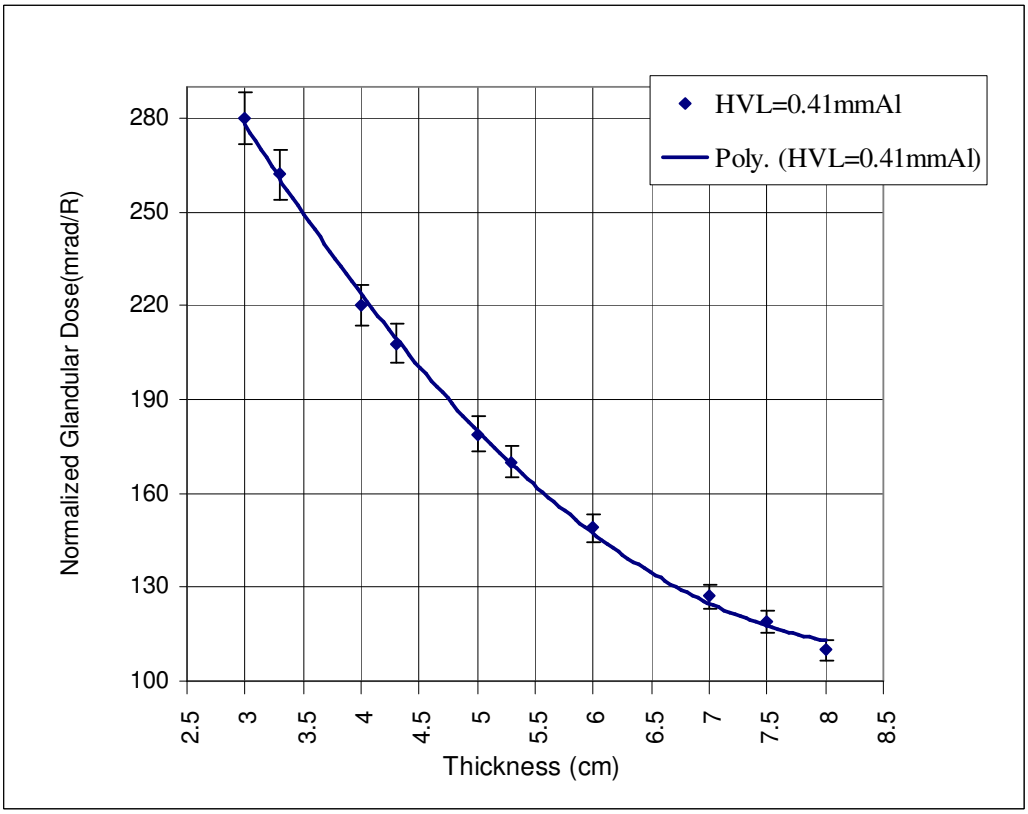

Figure 4.8 : Normalized glandular dose (mrad/R) at 32 kVp for Mo/Rh x-ray tube plotted as a function of depth for HVLs = 0.41 (mmAl)

The reason for having only one HVL=0.41mmAl in Figure 4.8 is because there were no data available in the literature.

4.1.2 Mean Glandular Dose

Finding the mean glandular dose, MGD, is the next step after interpolated D_{gN}. In this research our concern was a phantom with 7.5cm thickness. The D_{gN} values were inserted into equation 1 to find the mean glandular dose (MGD) for the 7.5cm thickness. This was done after measuring the entrance surface exposure (X_{ESE}) for each energy from both the Mo/Mo and the Mo/Rh target/filter combinations .

Using the D_{gN} values from Table 4.3 and inserting them into equation 1 produces Table 4.5 which has the MGD for the phantom thickness of 7.5cm for the x-ray energies used at different HVLs, for the Mo/Mo target/filter. In addition, to make sure that the entrance surface exposure is same for each kVp at different HVL, this study adjust the mAs for each kVp.

X-ray tube voltage, (kVp)	X_{ESE} (R)	Thickness (cm)	MGD (mGy)		
			HVL=0.29 (mmAl)	HVL=0.31 (mmAl)	HVL=0.35 (mmAl)
26	1.98	7.5	1.56	1.70	1.89
28	1.28	7.5	1.06	1.12	1.25
32	1.19	7.5	==	1.09	1.20

Table 4.5 : Mean glandular dose (MGD) at the phantom surface (thickness = 7.5 cm) for Mo/Mo target/filter x-ray tube for 26, 28, and 32 kVp

The unit used for the entrance surface exposure is "Roentgen" in Table 4.5, this was converted to SI units to find the MGD for each kVp in equation 1, which is designed to use Roentgen for X_{ESE}. Using Table 4.5 to study the changes in the MGD with the change of the beam quality for the same target/filter (Mo/Mo), can be plotted in Figure 4.9.

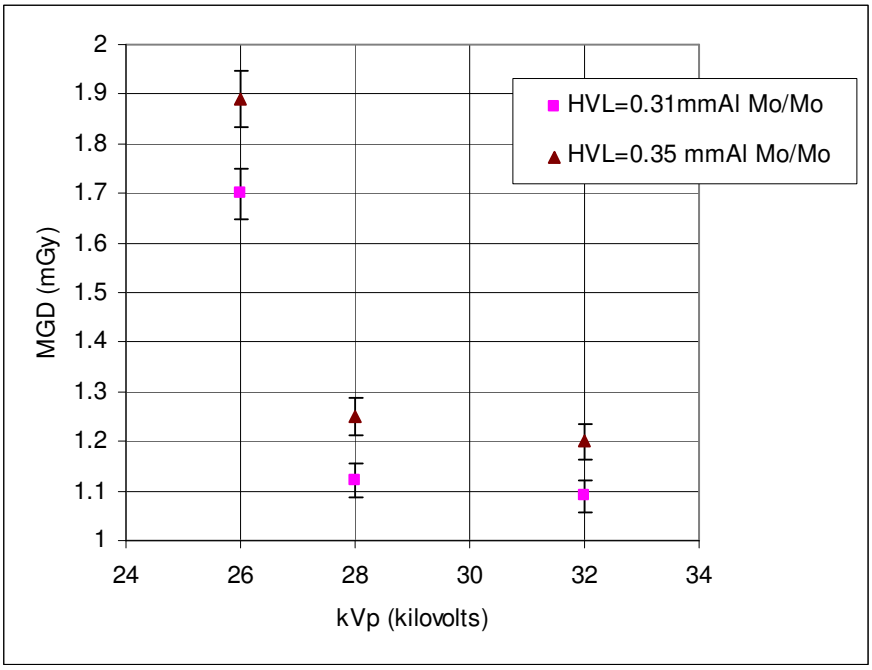

Figure 4.9 : The effect of the beam quality (HVL) on the mean glandular dose (MGD) for Mo/Mo target/filter.

Table 4.6 shows the MGD for the same phantom produced by using the D_{gN} of Mo/Rh target/filter combination in Table 4.4 after measuring the entrance surface dose and inserting both of the values in equation 1.

X-ray tube voltage, (kVp)	X_{ESE} (R)	Thickness (cm)	MGD (mGy)		
			HVL=0.36 (mmAl)	HVL=0.37 (mmAl)	HVL=0.41 (mmAl)
26	1.39	7.5	1.43	1.47	1.61
28	1.15	7.5	1.20	1.24	1.34
32	1.09	7.5	==	==	1.29

Table 4.6: Mean glandular dose (MGD) at the phantom surface (thickness = 7.5 cm) for Mo/Rh target/filter x-ray tube for 26, 28, and 32 kVp

Figure 4.10 shows the resulting relationship between kVp and MGD for one beam quality. Due to the time limitations more HVLs would have been covered.

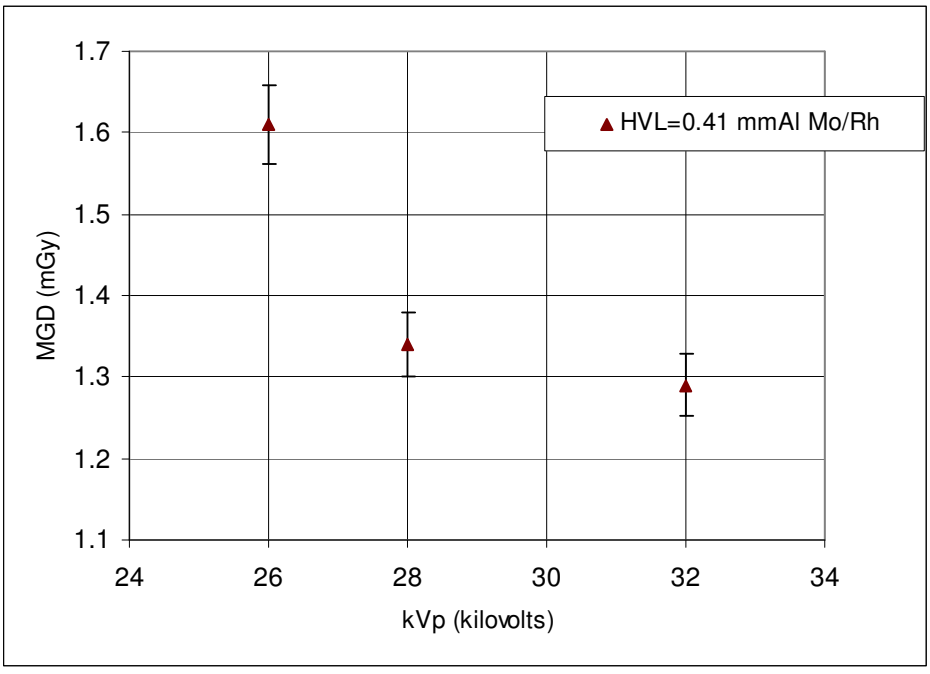

Figure 4.10 : The effect of the beam quality (HVL) on the mean glandular dose (MGD) for Mo/Rh target/filter.

4.2 Measuring the Dose as a function of Depth

TLDs were used to detect the dose at different depths inside the phantom, starting from the phantom surface to other depths of 3.3, 4.3 and 5.3cm.

After following the process of reading out all the TLDs measurements, this research compared the TLDs reading at each depth for each kVp, with the ionization chamber under the same conditions. The same process was followed for both target/filter combinations used in this research (Mo/Mo and Mo/Rh). Because the number of the TLDs was used at each depth (8 to 15) the average reading of the TLDs at each depth was used as the best value. Typically, TLDs give readings with a standard deviation around the mean of 3% [46], so an average reading is desirable. In other words, all the TLD readings with high standard deviations were excluded from the average calculations.

The TLDs readings at different kVps, surface and depths for the two target/filters used, can be found in Appendix A. One representative table is shown in Table 4.7

Depth = Surface, 26 kVp, 140 mAs					
Reading 1 (nC)	Reading 2 (nC)	Reading Average (nC)	Ionization chamber dose (mGy)	Calibration Factor (mGy/nC)	TLD Dose (mGy)
193.484	186.246	189.865	17.260	0.091	17.26 ± 0%
238.444	228.491	233.468	17.260	0.074	17.23 ± 3.0%
241.935	237.193	239.564	17.260	0.072	17. 24 ± 2.0%
247.682	240.346	244.014	17.260	0.071	17. 23 ± 3.0%
223.956	219.472	221.714	17.260	0.078	17.24 ± 2.0%
203.279	197.461	200.370	17.260	0.086	17.23 ± 3.0%
246.899	239.472	243.186	17.260	0.071	17.24 ± 2.0%
250.004	247.613	248.809	17.260	0.069	17.23 ± 3.0%
246.299	240.954	243.627	17.260	0.071	17. 24 ± 2.0%
238.528	231.746	235.137	17.260	0.073	17. 23 ± 3.0%
274.554	269.912	272.233	17.260	0.063	17. 24 ± 2.0%
263.56	259.461	261.511	17.260	0.066	17. 24 ± 2.0%
216.014	211.032	213.523	17.260	0.081	17. 23 ± 3.0%
251.772	249.347	250.560	17.260	0.069	17. 23 ± 3.0%

Table 4.7 : The TLDs reading at the phantom surface, using Mo/Mo, and 26 kVp

The last two columns in Table 4.7 need to be clarified. The calibration factor (CF) is a quantity that represents the amount of dose delivered to the detectors (TLDs) by (mGy) divided by the average of the detectors readings (nC) [46].

$$Calibration\ \ Factor \quad = \frac{dose\ delivered\ to\ the\ dosimeters\ (mGy)}{average\ dosimeter\ reading\ (nC)}$$

where the TLD dose represents the dose delivered to the TLDs after conversion into (mGy). This can be done by multiplying the calibration factor for each measurement with the average reading for each TLD [46].

$$TLD\ Dose = Calibration\ Factor \times Average\ reading\ \ for\ each\ TLD$$

The TLD dose average was used to represent the reading at kVp for each target/filter combination as a function of depth, with an uncertainty of 3%.

One of the goals in this research was to study the relationship between the changes in dose as a function of depth. Figures 4.11 and 4.12 show this relationship for each kVp for the two target/filter combinations used respectively.

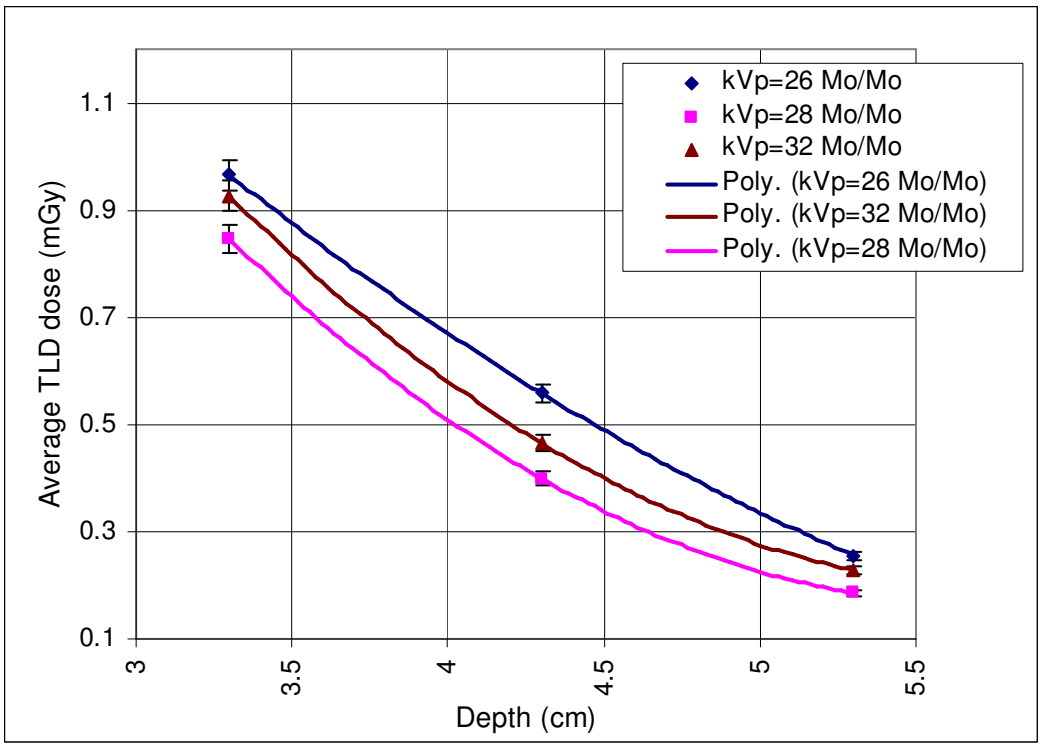

Figure 4.11 : The average TLD dose for Mo/Mo target/filter at 26, 28, and 32 kVp as a function of depth.

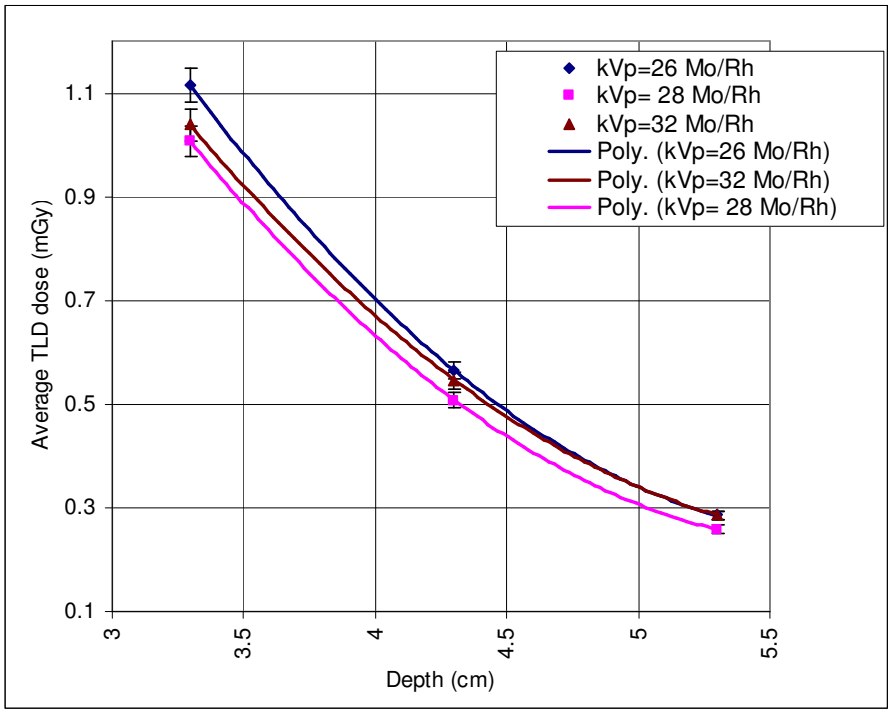

Figure 4.12 : The average TLD dose for Mo/Rh target/filter at 26, 28, and 32 kVp as a function of depth.

From the Tables 4.7 and 4.8-4.12 Appendix A, we can study the relation between the surface dose 7.5cm, as a function of the kVp for both target/filter combinations. Figure 4.13 shows this change as a comparison for the combinations target/filter used in this research.

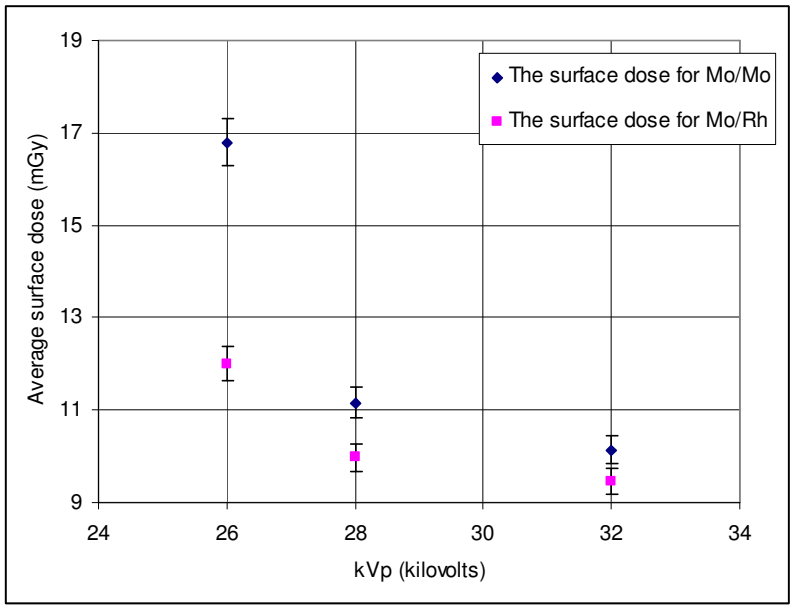

Figure 4.13 : The change on the surface dose for both Mo/Mo and Mo/Rh target/filter as a function of kVp.

5 Discussion and Conclusion

Figure 5.1 compares the results from this research (a) with the results from Wu X et al [22] (b). It shows the relationship between the x-ray tube voltage (kVp) and the beam quality (HVL) for a Mo target/ 0.03mm Mo filter and a Mo target/ 0.25mm Rh as a function of kVp. Note, this work's results values, include the attenuation of the compression paddle. This figure also shows what the HVL value depends on. The HVL value increases as kVp increases and the values for the Mo/Rh are higher than the Mo/Mo. This means the HVL depends on the atomic number of the target/filter used. The values from this research match well with the values from Wu X et al [22] in the Mo/Rh target/filter. It can be noted that the values work within the uncertainty for both. In the part of the Mo/Mo target/filter combination however, there is a difference with the measurements.

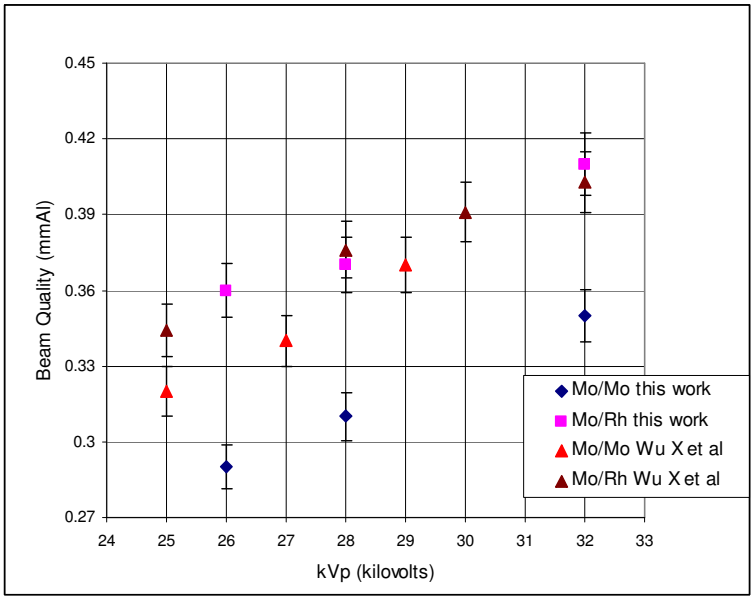

Figure 5.1 : The half value layer versus kVp for a Mo target/Mo filter and Mo target/Rh filter plotted as a function of kVp.

In this research, after measuring the HVL for the target/filter combinations used- Mo/Mo and Mo/Rh- the data presented in Tables 4.3 and 4.4 respectively, show the

values for the D_{gN} for different thicknesses. Combining these D_{gN} values for both filters, at each kVp, and plotting them as a function of depth to compare the change as the filters change, see Figures 5.2, 5.3 and 5.4.

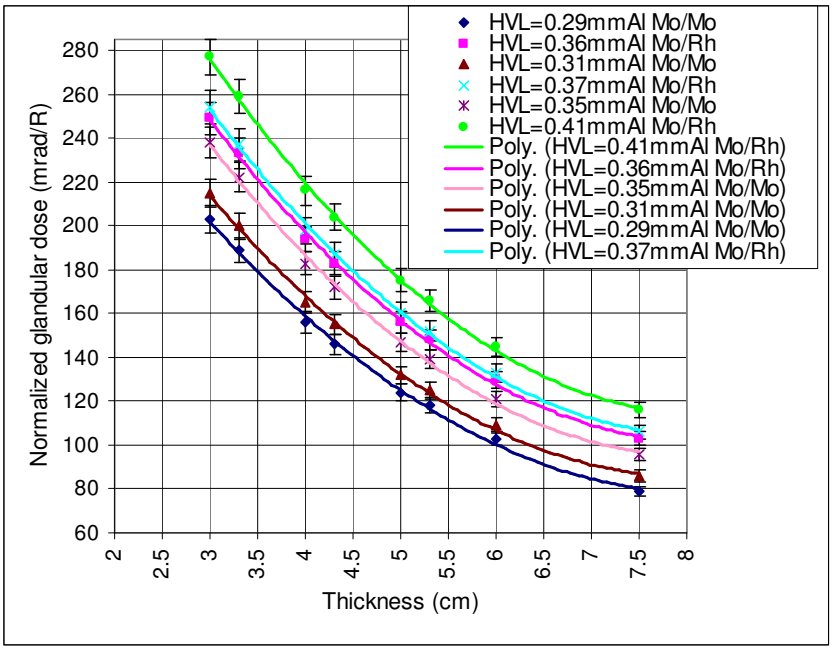

Figure 5.2 : Normalized glandular dose at 26 kVp, plotted as a function of 50/50 phantom for Mo/Mo and Mo/Rh target/filter x-ray tube

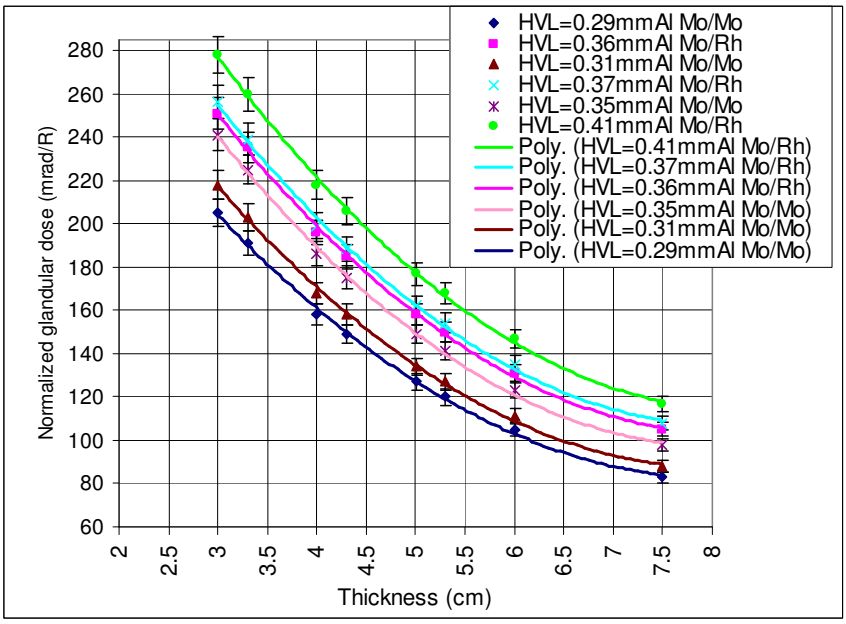

Figure 5.3 : Normalized glandular dose at 28 kVp, plotted as a function of 50/50 phantom for Mo/Mo and Mo/Rh target/filter x-ray tube.

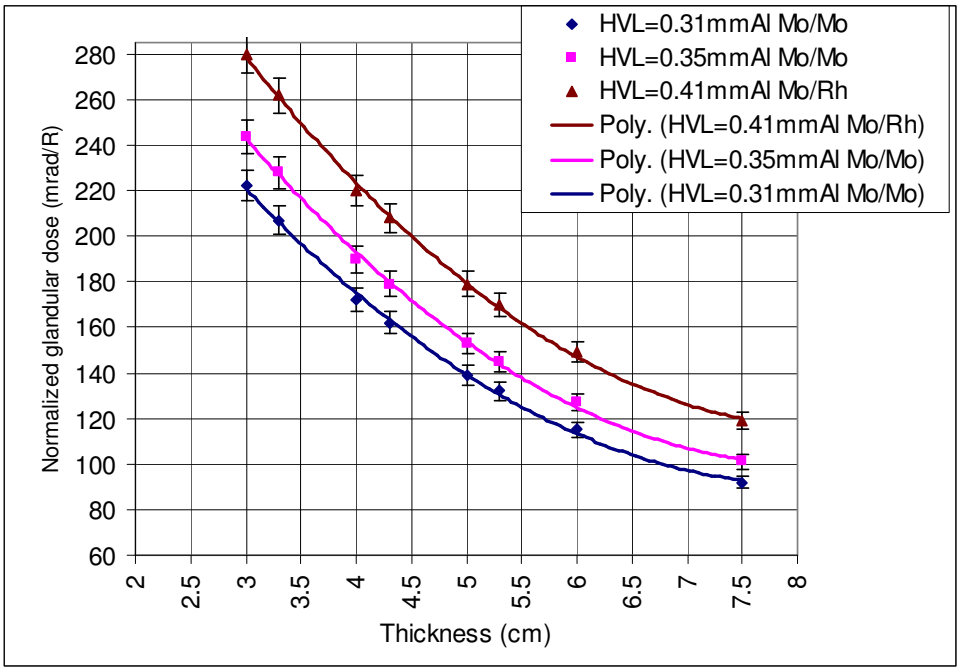

Figure 5.4 : Normalized glandular dose at 32 kVp, plotted as a function of 50/50 phantom for Mo/Mo and Mo/Rh target/filter x-ray tube.

As illustrated in Figures 5.2, 5.3 and 5.4, the normalized glandular dose increases as the HVL increases at the same depth, for the same target/filter combination. The D_{gN} values for the Mo/Rh are greater than the D_{gN} values using the Mo/Mo. This is considered a result of the spectra differences between the target/filter used. In other words, the Mo/Rh requires less entrance exposure dose X_{ESE} to achieve better image quality, without exposing the breast to a high surface exposure dose. It can also be seen from these figures that, as the thickness of the phantom increases, the normalized glandular dose decreases.

If we try to compare the results from this work with other researches, under the relationship between the phantom (breast) thickness and the normalized glandular dose, for one of the target/filter combinations (Mo/Mo) we will get this Figure 5.5.

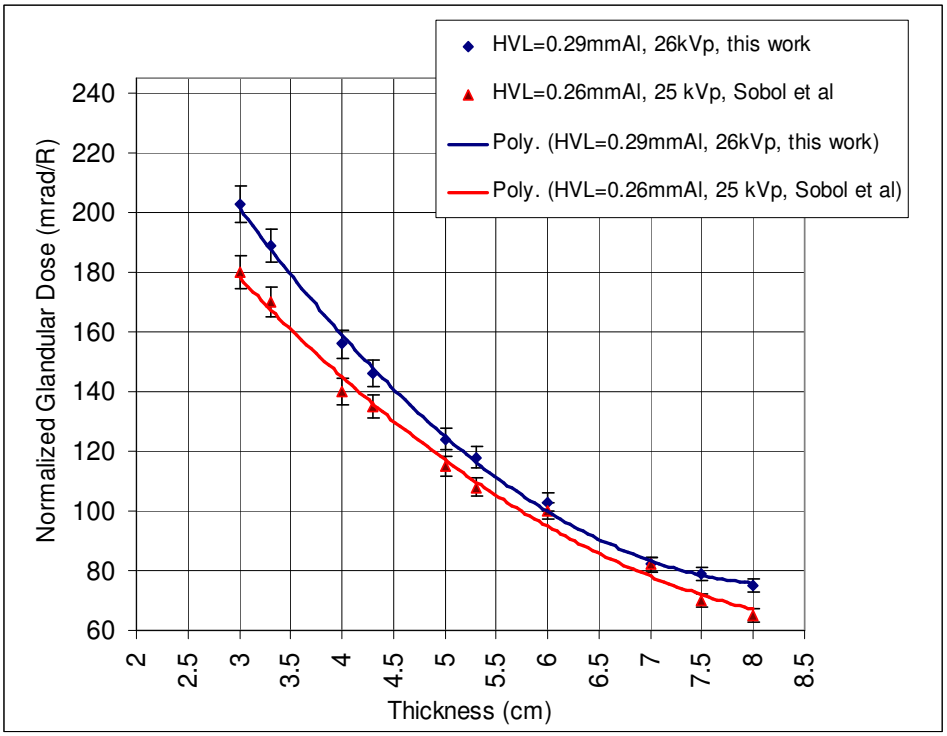

Figure 5.5 : Normalized glandular dose plotted as a function of 50/50 phantom for Mo/Mo target/filter x-ray tube. The curve in blue is from this work and the curve in red from Sobol et al work [58].

The results in Figure 5.5 show a good matching between this work and Sobol et al [58] work taking into consideration the difference of kVp and the HVL used.

Combining Figures 4.9 and 4.10 for the Mo/Mo and Mo/Rh target/filter respectively, to see the change on the MGD values as a function of the kVp, applied by different target/filter combinations at the phantom surface, can be seen in Figure 5.6.

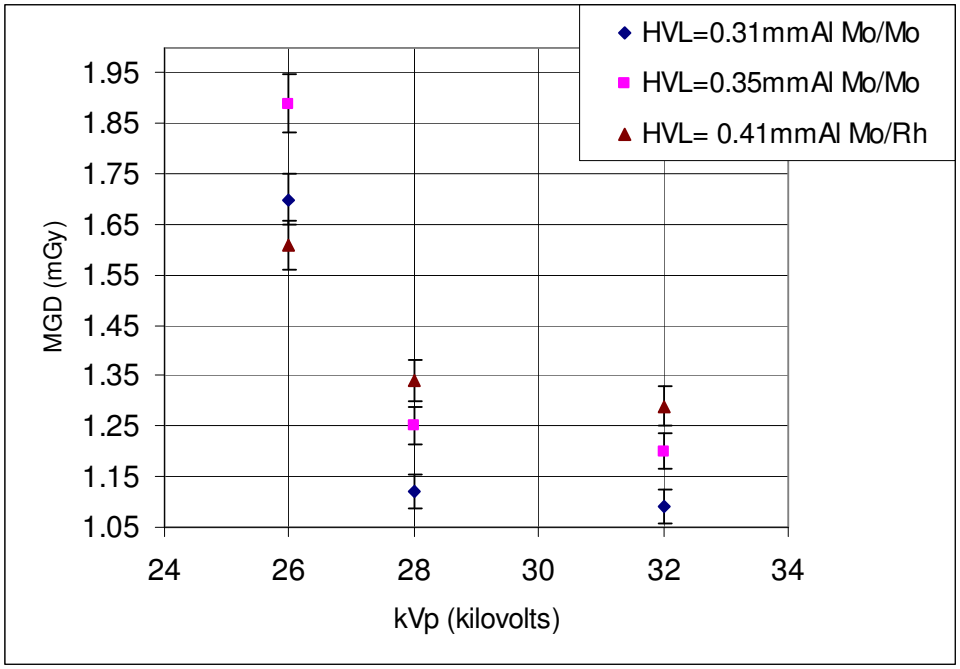

Figure 5.6 : Comparing the change on the MGD for a 7.5cm phantom thickness with the change of kVp for different HVLs at different target/filter combinations.

Looking at Figure 5.6, it can be seen that as the kVp increases at both target/filters, the D_{gN} decreases and as previously mentioned, the kVp increases the X_{ESE} decreases for both target/filter as well. Figure 5.6 shows the expectation from the Tables 4.5 and 4.6 that when the kVp increases, the MGD decreases resulting in the change in MGD values with Mo/Rh target/filter combination to be less steep than the change with Mo/Mo target/filter combination.

In addition the MGD values with the Mo/Rh target/filter are higher than the Mo/Mo, especially for higher kVp.

Figure 5.7 shows the Figures 4.11 and 4.12, where both show that as the depth increases, the dose decreases due to the increase of the attenuation of the x-ray beam inside the phantom.

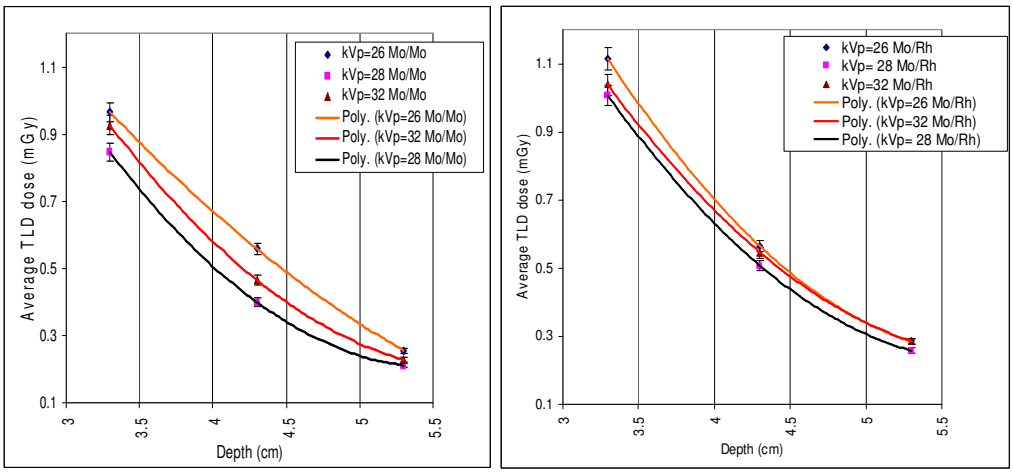

(a) (b)

Figure 5.7 : (a) Figure 4.11, (b) Figure 4.12.

Figures a and b show the average TLD dose at a specific depth dependence on the kVp used for the target/filter, where, as the kVp increases this value will decrease for the same depth.

In addition, we compared the relationship between the average TLDs dose as a function of depth for the Mo/Mo with the Mo/Rh target/filter. In Figures 4.11 and 4.12 it can be seen that the Mo/Rh values are higher than the Mo/Mo values at the same depth, for the same kVp value. This is due to the spectrum differences between the Mo/Mo and the Mo/Rh target/filter used. As mentioned before the Mo/Rh spectrum is higher than that of the Mo/Mo.

This research measured the dose at the surface of the phantom (breast). Figure 4.13 shows, the average of the TLD dose changes as a function of kVp. It is expected that the Mo/Mo target/filter has a higher entrance exposure dose X_{ESE} to achieve the better image quality. In other words it exposes the patient to less surface dose. Figure 4.13 shows that as the kVp value increases, the surface dose will decrease. This takes into consideration the spectral differences between the Mo/Mo and the Mo/Rh target/filter combinations, where the Mo/Rh target/filter has less entrance exposure dose than the

Mo/Mo target/filter at the same kVp. This shows the advantage of the Mo/Rh over the Mo/Mo target/filter, in terms of dose saving. Therefore, as the phantom thickness increases the penetrating ability of the Mo/Rh is higher than that of the Mo/Mo. The entrance exposure dose required is less than the Mo/Rh, therefore it is more dose saving. The penalty of having this advantage is in the image contrast. With the Mo/Rh, the image contrast is poor compared to the image produced using the Mo/Mo.

From the above, the dose expresses the energy deposited or absorbed in a specific tissue. In the breast, the glandular tissue is the radiosensitive tissue. Generally, the mean glandular dose is known as the reasonable quantity to represent the dose within the breast in regard to the risk of the ionizing radiation [61-63].

Measuring the MGD directly is not possible [7, 16]; therefore it requires measuring the entrance surface exposure and taking into consideration the breast thickness and composition [16, 21-22]. Because of that different models were created to understand the homogeneity of the breast tissue mixture. In other words, the glandular tissue composition inside the breast depends on different factors: the breast thickness and age [20, 64]. One of these models is the 50 glandular/50 fat tissues. This is considered to be the most appropriate model to represent the standard breast [16, 20]. However, this model is not an appropriate presentation of breasts with more than 6cm or less than 4cm thickness (less or more glandular tissue respectively). Age is not considered in this model [4, 25].

Therefore, measuring the dose delivered to the breast, as a function of depth, will give a better understanding for the mammography dose [16]. In this research, studying the

dose as a function of depth, did not take into consideration the different glandular tissue compositions within the breast, the age of the woman and the breast thickness. In addition, understanding the change of the dose inside the breast, will help to decide the upper limit for the surface dose in mammography which has not been confirmed by the International Atomic Energy Agency (IAEA) [4].

In conclusion, the mean glandular dose is the most common quantity used to represent the risk from the ionizing radiation used in the mammography screening, because of the sensitivity of the mammary glands. Measuring the MGD directly is not achievable, due to the need to measure the entrance surface exposure, taking into consideration the different factors which affect the MGD value-for example the kVp, target/filter combination, breast thickness and the beam quality (HVL).

The breast phantom models are designed to measure the MGD on the assumption that the breast mixture tissues, in a homogenous situation, without considering the effect of age and the thickness of the breast on the glandular tissue distribution within the breast.

IAEA states that MGD should be between (3-5) mGy for the average breast thickness. Women with a breast thickness smaller than the average breast thickness will receive a lower MGD, and those with a bigger breast thickness will receive higher a MGD [25].

On the other hand, measuring the change of the dose, as a function of depth, will provide a better understanding of the change of the dose inside the breast depending on the kVp, target/filter combination, beam quality and the entrance surface exposure.

Also, observing the change of the dose as a function of depth, can provide better calculation of the surface dose of mammography and therefore, reduce the risk of cancer from the mammography.

References

[1] National Breast Cancer Centre (2006, February). Advice about familial aspects of breast cancer and epithelial ovarian cancer. Retrieved from The National Breast Cancer Centre Website, Australia on 8 August 2007 at http://www.nbcc.org.au/resources/resource.php?code=BOG

[2] The National Cancer Institutes (NCI), (2006) available from: www.cancer.gov , accessed 12 March 2009

[3] The New Zealand Breast Cancer Foundation (2006), available from: www.nzbcf.org.nz , accessed 12 March 2009

[4] International Atomic Energy Agency (IAEA), Radiation Protection of Patients (RPoP), available from: www.rpop.iaea.rog , accessed 12 March 2009

[5] Ministry of Health/New Zealand Health Information Service (2006). Mortality and demographic data 2002 and 2003. p.25. Retrieved from The New Zealand National Screening Unit Website on 6 August 2007 at www.nzhis.govt.nz/publications/mortality.html

[6] Aznar, M. C., and Hemdal, B. A. Absorbed dose measurement in mammography. Cancer Imaging: Lung and Breast carcinomas

[7] Dance, D., Skinner, C., and Carlsson, G. Breast dosimetry. Applied Radiation and Isotopes 1999, vol. 50, pp. 185-203

[8] Heggie, J. C. P., McLean, I. Mammography physics & quality control. The University of Sydney, Faculty of Health Science

[9] Hall, E. Radiobiology for the radiologist. Fifth edition 2000

[10] Boone, J. Glandualr breast dose for monoenergetic and high-energy x-ray beams: Monte Carlo assessment. Radiology 1999, vol. 213, pp. 23-37

[11] Stanton, L., Villafana, T., Day, J. L., and Lightfoot, D. Dosage evaluation in mammography. Radiology 1984, vol. 150, pp. 577-584

[12] European Commission. European protocol on dosimetry in mammography. Report EUR 16263 (Bruxelles, Luxembourg: EC) 1996

[13] Dance, D., Skinner, C., Young, K., Beckett, J., and Kotre, C. Additional factors for estimation of mean glandular breast dose using the UK mammography dosimetry protocol. Phys. Med. Biol. 2000, vol. 45, pp. 3225-3240

[14] Klein, R., Aichinger, H., Dierker, J., Jansen, J. T., Joite-Barfu, S., Sabel, M., Schulz-Wendtland, R., and Zoetelief, J. Determination of average glandular dose with modern mammography units for two large groups of patients. Phys. Med. Biol. 1997, vol. 42, pp. 651-671

[15] Dance, D. Monte Carlo calculation of conversion factors for the estimation of mean glandular breast dose. Phys. Med. Biol.1990, vol. 35, pp. 1211-1219

[16] Hammerstein, G. R., Miller, D., White, D. R., Masterson, M., Woodard, H., and Laughlin, J. Absorbed radiation dose in mammography. Radiology 1979, vol. 130, pp. 485-491

[17] Delis, H., Spyrou, G., Panayiotakis, G., and Tzanakos, G. DOSIS: a Monte Carlo simulation program for dose related studies in mammography. European Journal of Radiology 2005, vol. 54, pp. 371-376

[18] Bushberg, J., Seibert, J., Leidholdt, E., and Boone, J. The essential physics of medical imaging. Second edition 2002

[19] Sookepeng, S., and Ketted, P. Mean glandular dose from routine mammography. Naresuan University Journal 2006, vol. 14, pp. 19-26

[20] Zankl, M., Fill, U., Hoeschen, C., Panzer, W. and Regulla, D. Average glandular dose conversion coefficints for segmented breast voxel models. Radiation Protection Dosimetry 2005, vol. 114, pp. 410-414

[21] Wu, X., Barnes, G. T., Tucker, and D. M. Spectral dependence of glandular tissue dose in screen-film mammography. Radiology 1991, vol. 179, pp. 143-148

[22] Wu, X., Gingold, E. L., Barnes, G., and Tucker, D. Normalized average glandular dose in molybdenum target-rhodium filter and rhodium target-rhodium filter mammography. Radiology 1994, vol. 193, pp. 83-89

[23] Martini, F., Nath, J. L. and Bartholomew, E. Fundamentals of anatomy & Physiology. Edition Eight, 2006

[24] Patrick, L. Breast normal anatomy cross-section, (2006), available from: http://patricklynch.net , accessed 12 March 2009

[25] Optimization of the radiological protection of patients: Image quality and dose in mammography (coordinated research in Europe). International Atomic Energy Agency (IAEA) 2005

[26] Heywang-Kobrunner, S., Dershaw, D., and Schreer, I. Diagnostic breast imaging: mammography, sonography, magnetic resonance imaging, and interventional procedures. Second edition 2001

[27] Faulkner, K., Law, J., and Robson, K. Assessment of mean glandular dose in mammography. The British Journal of Radiology, vol. 68, pp. 877-881

[28] The American Association of Physicts in Medicine, (2009), available from: www.aapm.org , accessed 12 March 2009

[29] Radiation Protection in Diagnostic and Interventional Radiology. International Atomic Energy Agency (IAEA). L19 Optimization of Protection in Mammography. Available from: www.rpop.iaea.org , accessed 12 March 2009

[30] Dance, D. A method for reconstruction of diagnostic x-ray spectra from measurements of attenuation. Phys. Med. Biol. 1987, vol. 32, pp. 1631-1638

[31] Jamal, N., and Mclean, D. A study of mean glandular dose during diagnostic mammography in Malaysia and some of the factors affecting it. The British Journal of Radiology 2003, vol. 76, pp. 238-245

[32] Mowlavi, A. X-ray spectra calculation for different target-filter of mammograms using MCNP code. Iran. J. Res. 2005, vol. 3, pp. 129-133

[33] Nishino, T., Wu, X., Johnson, R. Thickness of molybdenum filter and squared contrast-to-noise ratio per dose for digital mammography. Department of Radiology, University of Texas Medical Branch 2004

[34] Mammography quality control manual. American College of Radiology, Virginia 2002

[35] Matsumoto, M., Inoue, S., Honda, I., Yamamoto, S., Ueguchi, T., Ogata, Y. and Johkoh, T. Real-time estimation system for mean glandular dose in mammography. Radiation Medicine 2003, vol. 21, pp. 280-284

[36] Pages, J., and Van Loon, R. The European protocol on dosimetry in mammography: applicability and results in Belgium. Radiation Protection Dosimetry 1998, vol. 80, pp. 191-193

[37] The women's Health Resource, (1999) available from: www.imaginis.com , accessed 12 March 2009

[38] Perry, N., and Puthaar, E. European guidelines for quality assurance in breast cancer screening and diagnosis. Fourth edition 2006

[39] The 2007 Recommendations of the International Commission on Radiological Protection (Annuals of ICRP), Publication 103

[40] Warren-Forward, and H., Duggan, L. Towards *in vivo* TLD dosimetry in mammography. The British Journal of Radiology 2004, vol. 77, pp. 426-432

[41] Aznar, M. C. Real-time *in vivo* luminescence dosimetry in radiotherapy and mammography using Al_2O_3:C. RisØ-National Laboratory , Roskilde, Denmark 2005

[42] Gentry, J., and Dewerd, L. TLD measurements of in vivo Mammographic exposures and the calculated mean glandular dose across the United State. Medical Physics 1996, vol. 23, pp. 899-903

[43] National Cancer Institute (NCI), Final reports of the National Institute Cancer ad hoc working groups on mammography screening for breast cancer and a summary report of their joint findings and recommendations, 1977

[44] Faulkner, K., Broadhead, D., Harrison, R. Patient dosimetry measurement methods. Applied Radiation and Isotopes 1999, vol. 50, pp. 113-123

[45] Siemens Company, available from: www.medical.siemens.com , accessed 12 March 2009

[46] Mckinlay, A. F. Thermoluminescence dosimetry. Medical Physics Handbooks 1981, vol. 5

[47] Johns, H., and Gunningham, J. The physics of radiology. Fourth edition 1983

[48] Attix, F. Introduction to radiological physics and radiation dosimetry. 1986

[49] University of Gaziantep, Turkey, available from: www.gantep.edu , accessed 12 March 2009

[50] Miljanic, S., Ranogajec-Komor, M., and Vekic, B. Main dosimetric characteristics of some tissue-equivalent TL detectors. Radiation Protection Dosimetry 2002, vol. 100, pp. 437-442

[51] Taylor, G., and Lilley, E. The analysis of the thermolminescent glow peaks in LiF (TLD-100), J. Phys. D: Applied Physics. 1978, vol. 11, pp. 567-581

[52] Whall, M., and Roberts, P. Radiation dose in relation to compressed breast thickness for screening mammography. Radiation Protection Dosimetry 1992, vol. 43, pp. 253-255

[53] Hartley, L., Cobb, B., and Hutchinson, D. Estimating mean glandular dose using proprietary mammography phantoms. Applied Radiation and Isotopes 1999, vol. 50, pp. 205-213

[54] Collectible, Q. Mammography phantom image quality evaluation. Conference of Radiation Control Program Directors (CRCPD) 1996, pp. 1-7

[55] Fluke Biomedical Radiation Management Services, Fluke Biomedical Company, Virginia, United State of America. Model014A

[56] TRIAD Field Service Kit, Operator's Instruction Manual. Published (INOVSION) Radiation Measurements, Cleveland OH44139

[57] Thermo SCIENTIFIC, available from: www.thermo.com , accessed 12 March 2009

[58] W., Wu, X. Parametrization of mammography normalized average glandular dose tables. Medical Physics 1997, vol. 24, pp. 547-554

[59] Cranley, K., Gilmore, B. J., Foratry, G. W. A. and Desponds, L. Catalogue of diagnostic x-ray spectra & other data. IPEM Report 78 (Yourk: IPEM) 1997

[60] Skubic, S., and Fatouros, P. Absorbed breast dose: Dependence on radiographic modality and technique, and breast thickness. Radiology 1986, vol. 161, pp. 263-270

[61] Brenier, J., and Lisbona, A. Air Kerma calibration in mammography of thermoluminescence and semiconductor dosimeters against an ionization chamber. Radiation Protection Dosimetry 1998, vol. 80, pp. 239-241

[62] Kimme-Smith, C. New digital mammography systems may require different x-ray spectra and, therefore, more general normalized glandular dose values. Radiology 1999, vol. 213, pp. 7-10

[63] Nielsen, M., Gotzsche, PC. Screening for breast cancer with mammography (review). The Cochrane collaboration 2006

[64] Leitz, W. Design criteria for and evaluation of phantoms employed for mammography. Radiation Protection Dosimetry 1993, vol. 49, pp. 147-152

Mohammad Zeidan “Assessment of Mean Glandular Dose in Mammography” Poster presentation. The Engineering and Physical Sciences in Medicine and the Australian Biomedical Engineering 2008 Conference (epsm-abec 2008)

Appendix A

Tables

Depth = Surface, 28 kVp, 71mAs					
Reading 1 (nC)	Reading 2 (nC)	Reading Average (nC)	Ionization chamber dose (mGy)	Calibration Factor (mGy/nC)	TLD Dose (mGy)
132.087	130.792	131.440	11.230	0.085	11.230 ± 0%
120.643	115.972	118.308	11.230	0.095	11.210 ± 2.0%
158.889	152.647	155.768	11.230	0.072	11.198 ± 3.2%
123.85	120.091	121.971	11.230	0.092	11.216 ± 1.4%
165.118	170.41	167.764	11.230	0.067	11.210 ± 2.0%
182.34	176.494	179.417	11.230	0.063	11.209 ± 2.1%
172.884	168.002	170.443	11.230	0.066	11.210 ± 2.0%
161.029	158.135	159.582	11.230	0.070	11.200 ± 3.0%
147.623	142.764	145.194	11.230	0.077	11.206 ± 2.4%
160.429	152.138	156.284	11.230	0.072	11.215 ± 1.5%
180.17	176.843	178.507	11.230	0.063	11.209 ± 2.1%
177.64	174.084	175.862	11.230	0.064	11.213 ± 1.7%

Table 4.8: The TLDs reading at the phantom surface, using Mo/Mo, and 28 kVp.

Depth = Surface, 32 kVp, 45 mAs					
Reading 1 (nC)	Reading 2 (nC)	Reading Average (nC)	Ionization chamber dose (mGy)	Calibration Factor (mGy/nC)	TLD Dose (mGy)
143.582	139.462	141.522	10.410	0.074	10.410 ± 0%
155.813	148.327	152.070	10.410	0.068	10.373 ± 3.7%
156.16	161.012	158.586	10.410	0.066	10.369 ± 3.3%
145.278	139.487	142.383	10.410	0.073	10.384 ± 2.6%
143.94	137.648	140.794	10.410	0.074	10.372 ± 3.8%
166.009	157.913	161.961	10.410	0.064	10.369 ± 3.7%
148.975	140.681	144.828	10.410	0.072	10.379 ± 3.1%
165.917	158.698	162.308	10.410	0.064	10.386 ± 2.4%
148.447	139.741	144.094	10.410	0.072	10.382 ± 2.8%
174.11	167.852	170.981	10.410	0.061	10.378 ± 3.2%

Table 4.9: The TLDs reading at the phantom surface, using Mo/Mo, and 32kVp

Depth = Surface, 26 kVp, 125 mAs					
Reading 1 (nC)	Reading 2 (nC)	Reading Average (nC)	Ionization chamber dose (mGy)	Calibration Factor (mGy/nC)	TLD Dose (mGy)
175.609	169.403	172.506	12.130	0.070	12.130 ± 0%
186.789	180.579	183.684	12.130	0.066	12.102 ± 2.8%
189.5	182.359	185.930	12.130	0.065	12.105 ± 2.5%
169.139	164.487	166.813	12.130	0.073	12. 109 ± 2.1%
187.847	179.587	183.717	12.130	0.066	12.107 ± 2.3%
195.728	189.597	192.663	12.130	0.063	12.106 ± 2.4%
199.098	191.987	195.543	12.130	0.062	12.108 ± 2.2%
190.287	184.214	187.251	12.130	0.065	12.107 ± 2.3%
216.263	209.247	212.755	12.130	0.057	12.108 ± 2.2%
247.449	240.578	244.014	12.130	0.050	12.107 ± 2.3%
229.868	225.981	227.925	12.130	0.053	12.108 ± 2.2%
243.879	239.167	241.523	12.130	0.050	12.104 ± 2.6%
244.3	239.143	241.722	12.130	0.050	12.103 ± 2.7%

Table 4.10: The TLDs reading at the phantom surface, using Mo/Rh, and 26 kVp.

Depth = Surface, 28 kVp, 80 mAs					
Reading1 (nC)	Reading2 (nC)	Reading Average (nC)	Ionization chamber dose (mGy)	Calibration Factor (mGy/nC)	TLD Dose (mGy)
186.288	180.642	183.465	10.050	0.055	10.050 ± 0%
187.282	176.379	181.831	10.050	0.055	10.025 ± 2.5%
173.65	163.147	168.399	10.050	0.060	10.028 ± 2.2%
195.526	188.249	191.888	10.050	0.052	10.029 ± 2.1%
166.557	162.497	164.527	10.050	0.061	10.021 ± 2.9%
180.211	174.915	177.563	10.050	0.057	10.025 ± 2.5%
217.778	208.317	213.048	10.050	0.047	10.028 ± 2.2%
181.072	177.246	179.159	10.050	0.056	10.026 ± 2.4%
164.026	160.327	162.177	10.050	0.062	10.027 ± 2.3%
205.214	197.468	201.341	10.050	0.050	10.029 ± 2.1%
199.658	193.168	196.413	10.050	0.051	10.023 ± 2.7%
200.199	196.348	198.274	10.050	0.051	10.026 ± 2.4%
202.822	194.138	198.480	10.050	0.051	10.020 ± 3.0%
192.947	187.345	190.146	10.050	0.053	10.027 ± 2.3%

Table 4.11: The TLDs reading at the phantom surface, using Mo/Rh, and 28 kVp.

Depth = Surface, 32 kVp, 50 mAs					
Reading 1 (nC)	Reading 2 (nC)	Reading Average (nC)	Ionization chamber dose (mGy)	Calibration Factor (mGy/nC)	TLD Dose (mGy)
162.003	156.247	159.125	9.590	0.060	9.590 ± 0%
169.384	155.981	162.683	9.590	0.059	9.560 ± 3.0%
182.479	173.157	177.818	9.590	0.054	9.562 ± 2.8%
191.564	185.264	188.414	9.590	0.051	9.569 ± 2.1%
148.181	155.971	152.076	9.590	0.063	9.563 ± 2.7%
198.804	191.341	195.073	9.590	0.049	9.563 ± 2.7%
188.826	180.642	184.734	9.590	0.052	9.561 ± 2.9%
196.86	188.264	192.562	9.590	0.050	9.562 ± 2.8%
201.99	197.346	199.668	9.590	0.048	9.563 ± 2.7%
169.164	172.648	170.906	9.590	0.056	9.562 ± 2.8%
200.104	195.317	197.711	9.590	0.049	9.568 ± 2.2%

Table 4.12: The TLDs reading at the phantom surface, using Mo/Rh, and 32 kVp.

Depth = 5.3 cm, 26 kVp, 140 mAs					
Reading1 (nC)	Reading2 (nC)	Reading Average (nC)	Ionization chamber dose (mGy)	Calibration Factor (mGy/nC)	TLD Dose (mGy)
5.932	5.456	5.694	0.286	0.050	0.255 ± 3.1%
6.081	5.724	5.903	0.286	0.048	0.256 ± 3.0%
6.033	5.924	5.979	0.286	0.048	0.256 ± 3.0%
6.424	5.871	6.148	0.286	0.047	0.253 ± 3.3%
6.957	6.135	6.546	0.286	0.044	0.255 ± 3.1%
7.053	6.419	6.736	0.286	0.042	0.257 ± 2.9%
6.669	5.843	6.256	0.286	0.046	0.252 ± 3.4%
5.572	5.134	5.353	0.286	0.053	0.259 ± 2.7%
6.304	5.854	6.079	0.286	0.047	0.252 ± 3.4%
6.034	5.16	5.597	0.286	0.051	0.258 ± 2.8%
5.314	5.987	5.651	0.286	0.051	0.257 ± 2.9%
6.06	6.197	6.129	0.286	0.047	0.258 ± 2.8%

Table 4.13: The TLDs reading at 5.3 cm depth from the surface, using Mo/Mo, and 26 kVp.

Depth = 4.3 cm, 26 kVp, 140 mAs					
Reading 1 (nC)	Reading 2 (nC)	Reading Average (nC)	Ionization chamber dose (mGy)	Calibration Factor (mGy/nC)	TLD Dose (mGy)
11.579	11.235	11.407	0.583	0.051	0.583 ± 0%
11.556	10.891	11.224	0.583	0.052	0.553 ± 3.0%
13.735	12.672	13.204	0.583	0.044	0.553 ± 3.0%
11.896	10.924	11.410	0.583	0.051	0.555 ± 2.8%
10.744	10.397	10.571	0.583	0.055	0.556 ± 2.7%
14.084	14.571	14.328	0.583	0.041	0.557 ± 2.6%
13.213	12.843	13.028	0.583	0.045	0.559 ± 2.4%
13.078	12.137	12.608	0.583	0.046	0.555 ± 2.8%
13.141	12.896	13.019	0.583	0.045	0.559 ± 2.4%
12.856	12.597	12.727	0.583	0.046	0.554 ± 2.9%
12.898	12.972	12.935	0.583	0.045	0.556 ± 2.7%
13.342	12.951	13.147	0.583	0.044	0.555 ± 2.8%

Table 4.14: The TLDs reading at 4.3 cm depth from the surface, using Mo/Mo, and 26 kVp.

Depth = 3.3 cm, 26 kVp, 140 mAs					
Reading 1 (nC)	Reading 2 (nC)	Reading Average (nC)	Ionization chamber dose (mGy)	Calibration Factor (mGy/nC)	TLD Dose (mGy)
21.248	20.954	21.101	1.205	0.057	1.205 ± 0%
22.067	21.851	21.959	1.205	0.055	0.946 ± 2.6%
21.777	21.53	21.654	1.205	0.056	0.948 ± 2.6%
22.53	21.813	22.172	1.205	0.054	0.947 ± 2.6%
21.357	21.871	21.614	1.205	0.056	0.949 ± 2.6%
23.984	22.649	23.317	1.205	0.052	0.948 ± 2.6%
23.22	22.75	22.985	1.205	0.052	0.949 ± 2.6%
25.711	24.573	25.142	1.205	0.048	0.946 ± 2.7%
22.54	21.651	22.096	1.205	0.055	0.949 ± 2.7%
24.855	23.648	24.252	1.205	0.050	0.948 ± 2.6%
22.772	21.91	22.341	1.205	0.054	0.945 ± 2.6%
23.781	22.813	23.297	1.205	0.052	0.947 ± 2.6%
23.432	23.871	23.652	1.205	0.051	0.948 ± 2.7%
24.355	23.841	24.098	1.205	0.050	0.949 ± 2.6%
23.563	22.823	23.193	1.205	0.052	0.947 ± 2.6%

Table 4.15: The TLDs reading at 3.3 cm depth from the surface, using Mo/Mo, and 26 kVp.

Depth = 5.3 cm, 28 kVp, 71mAs					
Reading 1 (nC)	Reading 2 (nC)	Reading Average (nC)	Ionization chamber dose (mGy)	Calibration Factor (mGy/nC)	TLD Dose (mGy)
5.172	5.133	5.153	0.218	0.042	0.218 ± 0%
5.101	5.13	5.116	0.218	0.043	0.180 ± 3.8%
5.177	5.049	5.113	0.218	0.043	0.181 ± 3.7%
5.005	5.039	5.022	0.218	0.043	0.189 ± 2.9%
5.227	5.066	5.147	0.218	0.042	0.182 ± 3.6%
5.568	5.351	5.460	0.218	0.040	0.189 ± 2.9%
5.709	5.56	5.635	0.218	0.039	0.182 ± 3.6%
5.349	5.305	5.327	0.218	0.041	0.181 ± 3.7%
5.539	5.651	5.595	0.218	0.039	0.183 ± 3.5%
5.521	5.769	5.645	0.218	0.039	0.189 ± 2.9%
6.149	6.001	6.075	0.218	0.036	0.181 ± 3.7%
5.709	5.827	5.768	0.218	0.038	0.182 ± 3.6%

Table 4.16: The TLDs reading at 5.3 cm depth from the surface, using Mo/Mo, and 28 kVp.

Depth = 4.3 cm, 28 kVp, 71 mAs					
Reading 1 (nC)	Reading 2 (nC)	Reading Average (nC)	Ionization chamber dose (mGy)	Calibration Factor (mGy/nC)	TLD Dose (mGy)
8.293	8.082	8.188	0.429	0.052	0.429 ± 0%
8.602	8.182	8.392	0.429	0.051	0.399 ± 3.0%
9.904	9.515	9.710	0.429	0.044	0.396 ± 3.3%
8.578	8.143	8.361	0.429	0.051	0.397 ± 3.2%
7.945	7.519	7.732	0.429	0.055	0.397 ± 3.2%
10.111	9.736	9.924	0.429	0.043	0.396 ± 3.3%
9.405	9.544	9.475	0.429	0.045	0.399 ± 3.0%
9.193	9.313	9.253	0.429	0.046	0.397 ± 3.2%
9.399	9.363	9.381	0.429	0.046	0.395 ± 3.4%
9.111	9.143	9.127	0.429	0.047	0.398 ± 3.1%
9.133	9.14	9.137	0.429	0.047	0.395 ± 3.4%
9.74	9.833	9.787	0.429	0.044	0.396 ± 3.3%
10.013	9.97	9.992	0.429	0.043	0.397 ± 3.2%
10.073	10.103	10.088	0.429	0.043	0.399 ± 3.0%
8.5	8.551	8.526	0.429	0.050	0.397 ± 3.2%

Table 4.17: The TLDs reading at 4.3 cm depth from the surface, using Mo/Mo, and 28 kVp.

Depth = 3.3 cm, 28 kVp, 71 mAs					
Reading 1 (nC)	Reading 2 (nC)	Reading Average (nC)	Ionization chamber dose (mGy)	Calibration Factor (mGy/nC)	TLD Dose (mGy)
16.884	17.915	17.400	0.870	0.050	0.870 ± 0%
17.084	18.214	17.649	0.870	0.049	0.844 ± 2.6%
17.383	18.606	17.995	0.870	0.048	0.841 ± 2.9%
17.655	19.036	18.346	0.870	0.047	0.845 ± 2.5%
17.226	18.183	17.705	0.870	0.049	0.843 ± 2.7%
19.062	20.417	19.740	0.870	0.044	0.842 ± 2.8%
19.5	20.716	20.108	0.870	0.043	0.844 ± 2.6%
20.395	21.505	20.950	0.870	0.042	0.841 ± 2.9%

Table 4.18: The TLDs reading at 3.3 cm depth from the surface, using Mo/Mo, and 28 kVp.

Depth = 5.3 cm, 32 kVp, 45 mAs					
Reading 1 (nC)	Reading 2 (nC)	Reading Average (nC)	Ionization chamber dose (mGy)	Calibration Factor (mGy/nC)	TLD Dose (mGy)
6.034	5.431	5.7325	0.263	0.046	0.263 ± 0%
5.998	5.71	5.854	0.263	0.045	0.228 ± 3.5%
6.152	6.013	6.0825	0.263	0.043	0.225 ± 3.8%
6.137	5.73	5.9335	0.263	0.044	0.227 ± 3.6%
6.187	5.736	5.9615	0.263	0.044	0.225 ± 3.8%
6.252	6.004	6.128	0.263	0.043	0.226 ± 3.7%
6.665	6.279	6.472	0.263	0.041	0.223 ± 3.3%
6.548	6.197	6.3725	0.263	0.041	0.227 ± 3.6%
6.67	6.257	6.4635	0.263	0.041	0.224 ± 3.3%
6.801	6.249	6.525	0.263	0.040	0.228 ± 3.2%
7.403	6.73	7.0665	0.263	0.037	0.225 ± 3.4%
6.791	6.328	6.5595	0.263	0.040	0.226 ± 3.1%
6.254	5.653	5.9535	0.263	0.044	0.229 ± 3.4%
6.674	6.235	6.4545	0.263	0.041	0.229 ± 3.4%
6.467	5.794	6.1305	0.263	0.043	0.231 ± 3.2%

Table 4.19: The TLDs reading at 5.3 cm depth from the surface, using Mo/Mo, and 32 kVp.

Depth = 4.3 cm, 32 kVp, 45 mAs					
Reading 1 (nC)	Reading 2 (nC)	Reading Average (nC)	Ionization chamber dose (mGy)	Calibration Factor (mGy/nC)	TLD Dose (mGy)
9.844	9.647	9.7455	0.496	0.051	0.496 ± 0%
10.105	10.254	10.1795	0.496	0.049	0.465 ± 3.1%
11.694	11.941	11.8175	0.496	0.042	0.462 ± 3.4%
10.13	10.297	10.2135	0.496	0.049	0.463 ± 3.3%
9.04	8.901	8.9705	0.496	0.055	0.462 ± 3.4%
11.875	11.9	11.8875	0.496	0.042	0.463 ± 3.3%
11.326	11.519	11.4225	0.496	0.043	0.463 ± 3.3%
11.127	11.518	11.3225	0.496	0.044	0.461 ± 3.5%
11.387	11.649	11.518	0.496	0.043	0.460 ± 3.6%
10.814	11.124	10.969	0.496	0.045	0.463 ± 3.3%
10.458	10.745	10.6015	0.496	0.047	0.464 ± 3.2%
11.386	11.649	11.5175	0.496	0.043	0.462 ± 3.4%

Table 4.20: The TLDs reading at 4.3 cm depth from the surface, using Mo/Mo, and 32 kVp.

Depth = 3.3 cm, 32 kVp, 45 mAs					
Reading 1 (nC)	Reading 2 (nC)	Reading Average (nC)	Ionization chamber dose (mGy)	Calibration Factor (mGy/nC)	TLD Dose (mGy)
20.552	18.526	19.539	0.956	0.049	0.924 ± 3.2%
21.007	18.563	19.785	0.956	0.048	0.927 ± 2.9%
21.212	19.867	20.5395	0.956	0.047	0.926 ± 3.0%
20.285	18.525	19.405	0.956	0.049	0.924 ± 3.2%
22.25	20.354	21.302	0.956	0.045	0.925 ± 3.1%
22.933	20.654	21.7935	0.956	0.044	0.929 ± 2.7%
23.813	21.991	22.902	0.956	0.042	0.929 ± 2.7%
21.92	20.051	20.9855	0.956	0.046	0.921 ± 3.5%
22.239	20.746	21.4925	0.956	0.044	0.927 ± 2.9%
21.903	19.233	20.568	0.956	0.046	0.928 ± 2.8%
22.423	20.359	21.391	0.956	0.045	0.924 ± 3.2%
22.327	19.976	21.1515	0.956	0.045	0.927 ± 2.9%
22.827	20.117	21.472	0.956	0.045	0.925 ± 3.1%
22.028	19.61	20.819	0.956	0.046	0.928 ± 2.8%
19.88	17.372	18.626	0.956	0.051	0.926 ± 3.0%

Table 4.21: The TLDs reading at 3.3 cm depth from the surface, using Mo/Mo, and 32 kVp.

Depth = 5.3 cm, 26 kVp, 125 mAs					
Reading 1 (nC)	Reading 2 (nC)	Reading Average (nC)	Ionization chamber dose (mGy)	Calibration Factor (mGy/nC)	TLD Dose (mGy)
6.484	6.18	6.332	0.310	0.049	0.302 ± 2.8%
6.445	6.495	6.470	0.310	0.048	0.285 ± 2.5%
6.301	6.063	6.182	0.310	0.050	0.283 ± 2.7%
6.686	6.388	6.537	0.310	0.047	0.289 ± 2.1%
5.989	5.746	5.868	0.310	0.053	0.282 ± 2.8%
6.95	6.514	6.732	0.310	0.046	0.281 ± 2.9%
6.77	6.547	6.659	0.310	0.047	0.282 ± 2.8%
6.84	6.98	6.910	0.310	0.045	0.285 ± 2.5%
7.06	7.213	7.137	0.310	0.043	0.284 ± 2.6%
7.526	7.572	7.549	0.310	0.041	0.281 ± 2.9%
7.129	7.138	7.134	0.310	0.043	0.284 ± 2.6%
6.304	6.165	6.235	0.310	0.050	0.281 ± 2.9%

Table 4.22: The TLDs reading at 5.3 cm depth from the surface, using Mo/Rh, and 26 kVp.

Depth = 4.3 cm, 26 kVp, 125 mAs					
Reading 1 (nC)	Reading 2 (nC)	Reading Average (nC)	Ionization chamber dose (mGy)	Calibration Factor (mGy/nC)	TLD Dose (mGy)
11.457	11.467	11.462	0.592	0.052	0.572 ± 2.0%
12.051	12.154	12.103	0.592	0.049	0.565 ± 2.7%
14.216	14.191	14.204	0.592	0.042	0.568 ± 2.4%
11.864	11.735	11.800	0.592	0.050	0.560 ± 3.2%
10.777	10.612	10.695	0.592	0.055	0.567 ± 2.5%
14.078	14.376	14.227	0.592	0.042	0.564 ± 2.8%
13.456	13.452	13.454	0.592	0.044	0.562 ± 3.0%
13.235	13.581	13.408	0.592	0.044	0.566 ± 2.6%
13.547	13.956	13.752	0.592	0.043	0.566 ± 2.6%
13.436	13.342	13.389	0.592	0.044	0.560 ± 3.2%
12.774	13.065	12.920	0.592	0.046	0.561 ± 3.1%
13.839	13.912	13.876	0.592	0.043	0.565 ± 2.7%
14.426	14.926	14.676	0.592	0.040	0.562 ± 3.0%

Table 4.23: The TLDs reading at 4.3 cm depth from the surface, using Mo/Rh, and 26 kVp.

Depth = 3.3 cm, 26 kVp, 125 mAs					
Reading 1 (nC)	Reading 2 (nC)	Reading Average (nC)	Ionization chamber dose (mGy)	Calibration Factor (mGy/nC)	TLD Dose (mGy)
21.787	20.812	21.300	1.144	0.054	1.144 ± 0%
21.38	20.7	21.040	1.144	0.054	1.113 ± 3.1%
21.739	20.606	21.173	1.144	0.054	1.112 ± 3.2%
22.552	21.971	22.262	1.144	0.051	1.114 ± 3.0%
20.913	19.918	20.416	1.144	0.056	1.115 ± 2.9%
23.508	22.549	23.029	1.144	0.050	1.112 ± 3.2%
23.366	22.138	22.752	1.144	0.050	1.111 ± 3.3%
25.415	24.996	25.206	1.144	0.045	1.113 ± 3.1%
22.317	21.385	21.851	1.144	0.052	1.112 ± 3.2%
24.317	24.479	24.398	1.144	0.047	1.114 ± 3.0%
21.853	21.382	21.618	1.144	0.053	1.115 ± 2.9%
23.196	22.801	22.999	1.144	0.050	1.116 ± 2.8%
22.982	22.908	22.945	1.144	0.050	1.112 ± 3.2%
23.589	23.239	23.414	1.144	0.049	1.110 ± 3.4%

Table 4.24: The TLDs reading at 3.3 cm depth from the surface, using Mo/Rh, and 26 kVp.

Depth = 5.3 cm, 28 kVp, 80 mAs					
Reading 1 (nC)	Reading 2 (nC)	Reading Average (nC)	Ionization chamber dose (mGy)	Calibration Factor (mGy/nC)	TLD Dose (mGy)
5.832	5.665	5.749	0.286	0.050	0.257 ± 2.9%
6.009	5.73	5.870	0.286	0.049	0.258 ± 2.8%
5.892	5.732	5.812	0.286	0.049	0.259 ± 2.7%
6.159	5.713	5.936	0.286	0.048	0.257 ± 2.9%
5.219	5.245	5.232	0.286	0.055	0.257 ± 2.9%
6.084	5.825	5.955	0.286	0.048	0.259 ± 2.7%
5.839	5.843	5.841	0.286	0.049	0.258 ± 2.8%
6.284	5.975	6.130	0.286	0.047	0.259 ± 2.7%
6.263	5.911	6.087	0.286	0.047	0.259 ± 2.7%
6.994	6.551	6.773	0.286	0.042	0.257 ± 2.9%
6.709	6.436	6.573	0.286	0.044	0.258 ± 2.8%
5.536	5.108	5.322	0.286	0.054	0.257 ± 2.9%
6.31	6.012	6.161	0.286	0.046	0.259 ± 2.7%
5.799	5.646	5.723	0.286	0.050	0.256 ± 3.0%

Table 4.25: The TLDs reading at 5.3 cm depth from the surface, using Mo/Rh, and 28 kVp.

Depth = 4.3 cm, 28 kVp, 80 mAs					
Reading 1 (nC)	Reading 2 (nC)	Reading Average (nC)	Ionization chamber dose (mGy)	Calibration Factor (mGy/nC)	TLD Dose (mGy)
10.509	10.715	10.612	0.536	0.051	0.536 ± 0%
10.51	10.952	10.731	0.536	0.050	0.508 ± 2.8%
12.594	12.827	12.711	0.536	0.042	0.509 ± 2.7%
10.903	10.672	10.788	0.536	0.050	0.501 ± 3.5%
9.63	9.812	9.721	0.536	0.055	0.509 ± 2.7%
12.655	12.951	12.803	0.536	0.042	0.506 ± 3.0%
12.308	12.468	12.388	0.536	0.043	0.509 ± 2.7%
11.982	12.641	12.312	0.536	0.044	0.502 ± 3.4%
12.382	12.758	12.570	0.536	0.043	0.503 ± 3.3%
12.167	12.206	12.187	0.536	0.044	0.501 ± 3.5%
11.719	12.092	11.906	0.536	0.045	0.508 ± 2.8%
12.695	12.541	12.618	0.536	0.042	0.501 ± 3.5%
13.405	13.094	13.250	0.536	0.040	0.502 ± 3.4%

Table 4.26: The TLDs reading at 4.3 cm depth from the surface, using Mo/Rh, and 28 kVp.

Depth = 3.3 cm, 28 kVp, 80 mAs					
Reading 1 (nC)	Reading 2 (nC)	Reading Average (nC)	Ionization chamber dose (mGy)	Calibration Factor (mGy/nC)	TLD Dose (mGy)
17.987	18.528	18.258	1.033	0.057	1.033 ± 0%
18.342	18.247	18.295	1.033	0.056	1.001 ± 3.2%
17.925	18.661	18.293	1.033	0.056	1.004 ± 2.9%
19.792	19.981	19.887	1.033	0.052	1.003 ± 3.0%
17.654	17.719	17.687	1.033	0.058	1.006 ± 2.7%
20.774	20.524	20.649	1.033	0.050	1.003 ± 3.0%
19.783	19.503	19.643	1.033	0.053	1.009 ± 2.4%
21.981	22.455	22.218	1.033	0.046	1.002 ± 3.1%
18.561	19.041	18.801	1.033	0.055	1.003 ± 3.0%
21.398	21.878	21.638	1.033	0.048	1.002 ± 3.1%
18.506	18.279	18.393	1.033	0.056	1.005 ± 2.8%
20.118	20.128	20.123	1.033	0.051	1.007 ± 2.6%

Table 4.27: The TLDs reading at 3.3 cm depth from the surface, using Mo/Rh, and 28 kVp.

Depth = 5.3 cm, 32kVp, 50 mAs					
Reading 1 (nC)	Reading 2 (nC)	Reading Average (nC)	Ionization chamber dose (mGy)	Calibration Factor (mGy/nC)	TLD Dose (mGy)
6.401	6.357	6.379	0.314	0.049	0.304 ± 1.0%
6.443	6.243	6.343	0.314	0.050	0.285 ± 2.9%
6.133	6.167	6.150	0.314	0.051	0.286 ± 2.8%
6.385	6.065	6.225	0.314	0.050	0.283 ± 3.1%
5.605	5.569	5.587	0.314	0.056	0.284 ± 3.0%
6.644	6.532	6.588	0.314	0.048	0.283 ± 3.1%
6.74	6.298	6.519	0.314	0.048	0.285 ± 2.9%
6.682	6.554	6.618	0.314	0.047	0.284 ± 3.0%
6.835	6.41	6.623	0.314	0.047	0.284 ± 3.0%
7.226	7.215	7.221	0.314	0.043	0.283 ± 3.1%
7.028	6.957	6.993	0.314	0.045	0.284 ± 3.0%
5.668	5.719	5.694	0.314	0.055	0.286 ± 2.8%
6.81	6.396	6.603	0.314	0.048	0.285 ± 2.9%
6.024	5.816	5.920	0.314	0.053	0.284 ± 3.0%

Table 4.28: The TLDs reading at 5.3 cm depth from the surface, using Mo/Rh, and 32 kVp

Depth = 4.3 cm, 32kVp, 50 mAs					
Reading 1 (nC)	Reading 2 (nC)	Reading Average (nC)	Ionization chamber dose (mGy)	Calibration Factor (mGy/nC)	TLD Dose (mGy)
11.227	11.283	11.255	0.572	0.051	0.572 ± 0%
11.927	12.18	12.054	0.572	0.047	0.544 ± 2.8%
14.06	13.945	14.003	0.572	0.041	0.542 ± 3.0%
11.722	12.012	11.867	0.572	0.048	0.546 ± 2.6%
10.256	10.768	10.512	0.572	0.054	0.543 ± 2.9%
13.781	14.231	14.006	0.572	0.041	0.543 ± 2.9%
13.573	13.604	13.589	0.572	0.042	0.544 ± 2.8%
13.554	13.739	13.647	0.572	0.042	0.542 ± 3.0%
13.633	13.742	13.688	0.572	0.042	0.544 ± 2.8%
12.697	13.238	12.968	0.572	0.044	0.546 ± 2.6%
12.677	12.903	12.790	0.572	0.045	0.543 ± 2.9%
13.517	13.698	13.608	0.572	0.042	0.549 ± 2.3%
14.347	14.665	14.506	0.572	0.039	0.543 ± 2.9%

Table 4.29: The TLDs reading at 4.3 cm depth from the surface, using Mo/Rh, and 32 kVp.

Depth = 3.3 cm, 32 kVp, 50 mAs					
Reading 1 (nC)	Reading 2 (nC)	Reading Average (nC)	Ionization chamber dose (mGy)	Calibration Factor (mGy/nC)	TLD Dose (mGy)
18.82	19.072	18.946	1.066	0.056	1.066 ± 0%
19.114	19.045	19.080	1.066	0.056	1.038 ± 2.8%
19.333	19.363	19.348	1.066	0.055	1.034 ± 3.2%
20.469	20.225	20.347	1.066	0.052	1.038 ± 2.8%
18.031	17.757	17.894	1.066	0.060	1.039 ± 2.7%
20.603	20.423	20.513	1.066	0.052	1.036 ± 3.0%
19.46	19.38	19.420	1.066	0.055	1.038 ± 2.8%
22.719	22.851	22.785	1.066	0.047	1.031 ± 3.5%
19.126	18.534	18.830	1.066	0.057	1.039 ± 2.7%
22.271	21.661	21.966	1.066	0.049	1.036 ± 3.0%
17.928	17.983	17.956	1.066	0.059	1.039 ± 2.7%
20.382	19.667	20.025	1.066	0.053	1.032 ± 3.4%
20.42	20.165	20.293	1.066	0.053	1.039 ± 2.7%
21.352	21.136	21.244	1.066	0.050	1.032 ± 3.4%

Table 4.30: The TLDs reading at 3.3 cm depth from the surface, using Mo/Rh, and 32 kVp.